biophysica

MDPI

Review

Evaporation-Driven Self-Assembly and Deposition Patterns of Protein Droplets: Mechanisms, Modulation, and Applications

Xuanyi Zhang [1,*], Zehua Wang [2], Chenyang Wu [1] and Dongdong Lin [1,*]

[1] School of Physical Science and Technology, Ningbo University, 818 Fenghua Road, Ningbo 315211, China
[2] Ningbo Institute of Digital Twin, Eastern Institute of Technology, Ningbo 315200, China
* Correspondence: 236002705@nbu.edu.cn (X.Z.); lindongdong@nbu.edu.cn (D.L.)

Abstract

Protein droplets exhibit complex self-assembly and deposition behaviors driven by evaporation, which has attracted increasing attention in recent years. Under evaporation, limited volume and locally concentrated protein solutions can undergo liquid–liquid phase separation (LLPS) and liquid–liquid crystalline phase separation (LLCPS), inducing the formation of concentrated droplets and anisotropic structures. The combined effects of interfacial tension and internal flow field induce a variety of deposition patterns on the substrate, providing great significance for the development of functional biomaterials. This paper reviews the physical processes experienced by protein/fibril droplets during evaporation, focusing on the formation mechanism of evaporation and their phase separation behaviors. At the same time, the review systematically summarized the key factors affecting the deposition patterns, and a variety of methods were introduced to pattern deposition, such as external electric field and micro-structured substrates. Furthermore, the potential applications of proteins/fibrils droplet deposition were discussed in multiple fields. This review aims to provide systematic theoretical support and experimental reference for understanding and controlling the deposition behavior of proteins/fibrils droplets, and to promote their further application in functional materials and biomedical engineering.

Keywords: evaporation; self-assembly; phase separation; deposition; fibrils

check for updates

Academic Editor: Javier Sancho

Received: 24 September 2025
Revised: 5 November 2025
Accepted: 8 November 2025
Published: 21 November 2025

Citation: Zhang, X.; Wang, Z.; Wu, C.; Lin, D. Evaporation-Driven Self-Assembly and Deposition Patterns of Protein Droplets: Mechanisms, Modulation, and Applications. *Biophysica* **2025**, *5*, 57. https://doi.org/10.3390/biophysica5040057

Copyright: © 2025 by the authors. Licensee MDPI, Basel, Switzerland. This article is an open access article distributed under the terms and conditions of the Creative Commons Attribution (CC BY) license (https://creativecommons.org/licenses/by/4.0/).

1. Introduction

Amyloids, a type of fibrillar aggregated with highly ordered β-pleated structures [1], are widely present in nature and are associated with a variety of neurodegenerative diseases [2]. In recent years, they have gradually demonstrated great potential for application in nanomaterials [3–7], bio-interfaces [8–12], flexible electronics [13–16], and functional coatings [17–19]. As an emerging and highly dynamic research field, functional amyloid materials have expanded our understanding of the properties of protein materials in new and unexpected way. During the evaporation of the solution, amyloid proteins/fibrils exhibit unique undergo liquid–liquid phase separation (LLPS) and liquid–liquid crystalline phase separation (LLCPS) behavior and directional self-assembly ability [20,21]. Under the coupling of limited volume, non-uniform concentration and interfacial tension, they can form highly ordered droplets and various deposition patterns [22,23]. This type of evaporation-driven self-assembly process not only provides a green and environmentally friendly way to construct structures but also provides a new perspective for revealing the interfacial behavior and directional self-assembly mechanism of protein materials.

Scientists have discovered that colloidal droplets exhibit a variety of deposition patterns during the drying process, such as rings [24], spirals [25], web [26], or concentric structures [27]. The formation of these deposition patterns is related to fluid dynamics, interface physics, and the orientation and agglomerability of the colloidal particles themselves. At the same time, the regulation strategies are becoming increasingly diverse that from the earliest adjustments to the concentration and temperature of the solution to the application of external electric fields, addition of surfactants, design of micro-structural substrates, and surface functionalization. These studies have greatly enriched the strategy of regulating protein fibril deposition behavior [28–33]. Although there are many reports on the evaporation deposition mechanism and regulation methods, there is still a lack of systematic reviews on the special system of proteins/fibrils droplets. In particular, the structural evolution process of droplets dominated by LLCPS and LLCPS, the precise control methods of deposition patterns and the practical application of structured deposition still need to be further sorted out and summarized.

This review aims to comprehensively summarize the self-assembly behavior and deposition patterns induced by evaporation-driven proteins/fibrils droplets, focusing on the evolutionary mechanisms of their phase behavior and strategies for regulating deposition patterns. It also explores their potential applications in nanostructure construction, biomedicine and flexible applications. Finally, the article will consider current research challenges and explore future research directions in cross-scale assembly methods, multifunctional interface construction, and bio-system integration.

2. Fundamentals of Evaporation and Deposition Processes

2.1. Mechanism of Evaporation-Induced Phase Separation

During evaporation, proteins/fibrils droplets undergo a transition from a liquid state to a deposited pattern. The internal flow field driven by evaporation causes the migration and accumulation of colloidal particles [22]. This accumulation of particles also affects the phase behavior of the proteins/fibrils. The coupling of multiple mechanisms ultimately results in a diverse array of deposited patterns [34]. During the evaporation of a droplet, the evaporation rate at the edge (near the contact line) is higher than that at the center. Therefore, to compensate for the liquid loss near the contact line, a capillary compensation flow will form inside the droplet from the center to the edge (Figure 1a) [35]. This flow will transport proteins/fibrils or other solute particles in the solution to the edge of the droplet, thereby forming a typical ring-shaped deposition structure. This phenomenon is called coffee ring effect, as shown in Figure 1b [24]. This process usually occurs in the constant contact area mode [36]. As shown in Figure 1c [37], the contact line remains pinned during the evaporation of the droplet, that is, the contact area between the droplet and the substrate remains unchanged during the evaporation process. In this mode, flows caused by geometric constraints will appear inside the droplet to compensate for the liquid volume lost due to edge evaporation. These flows not only determine the transport path of the particles, but also directly affect the final deposition pattern. In the constant contact angle mode [36], the contact angle of the droplet remains constant, while the contact line (i.e., the edge of the droplet and the substrate) gradually shrinks toward the center as the volume of the liquid decreases (Figure 1d). This shrinkage process means that the bottom area of the droplet is gradually getting smaller, and the droplet volume is reduced proportionally to maintain the initial contact angle. In this mode, the internal flow and solute migration path caused by evaporation also change. As the contact line continues to move inward, the liquid replenishment demand caused by evaporation occurs in the entire retracting contact line area. It will induce an inward flow from the edge to the center of the liquid, which is opposite to the outward capillary flow in the constant contact area mode. It will

induce solutes (such as protein fibrils, colloidal particles, etc.) gradually enrich toward to the center of the droplet, eventually forming a central deposition structure, rather than the typical coffee ring edge deposition.

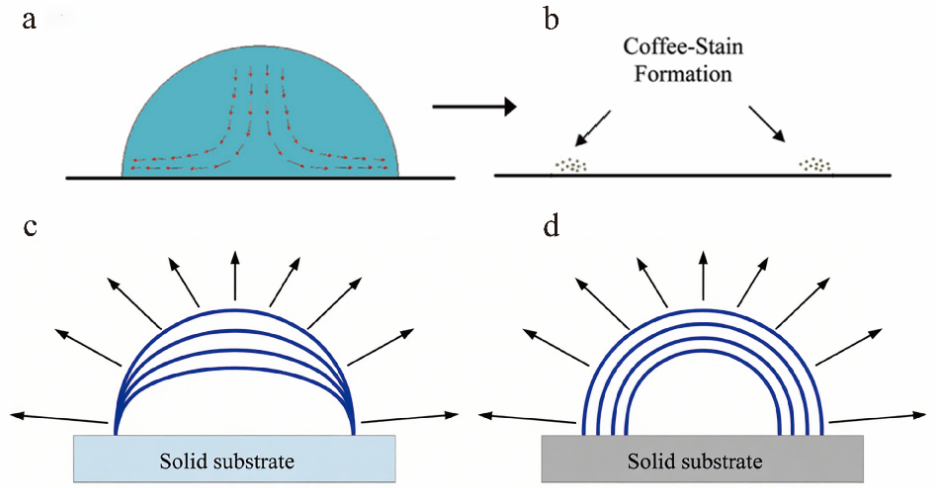

Figure 1. Capillary flow and two evaporation modes of droplets. (**a**,**b**) Particle motion within a droplet under standard ambient evaporation conditions shows that the difference in evaporation rates between the edge and the center drives particles toward the edge, leading to the formation of coffee stains, in (**a**), the red dashed arrows indicate the direction of fluid flow, and the black arrows indicate the sequence of process steps. In (**b**), the downward arrows indicate the direction of deposition. (**c**) Constant contact line mode (CCR) and (**d**) constant contact angle mode (CCA). The arrows in (**c**) and (**d**) indicate the direction in which the solute (water) in the droplet evaporates outward. [35,37].

2.2. LLPS and LLCPS

Both LLPS [38,39] and LLCPS [23,40] arise from instabilities in the free energy of the system. They share similarities in their thermodynamic frameworks. Both can describe phase coexistence through conditions of equality between chemical potential and osmotic pressure, and the dynamic evolution of the two types of phase separation follows similar pathways, namely nucleation and growth or spiny nucleation decomposition that separates the dilute and concentrated phases. However, the underlying physics underlying the theoretical framework defining LLCPS is completely different from the physics of LLPS [41].

LLPS is primarily described within the Flory-Huggins theoretical framework [42], based on a balance between mixing entropy and interaction energy [43]. In the Flory-Huggins theory, mixing entropy primarily originates from the arrangement of polymer chains on a lattice model. For polymer solutions, entropy contributions stem from the chain's translational and configurational degrees of freedom. LLCPS is mainly described by the Onsager theory framework [44]. When many long and thin rigid rod-like particles are present in the solution, the system will undergo an anisotropic ordering transition at a certain concentration. At low concentrations, the rods are randomly oriented (isotropic phase). When a certain concentration threshold is reached, the rods tend to be arranged in parallel (nematic phase) [45]. The theory shows that this ordering transition is not driven by intermolecular attraction, but is purely caused by repulsion and entropy effects. It describes the formation of ordered phases in rigid particle systems caused by the competition between exclusion volume and orientation entropy.

LLCPS is a common phenomenon in rigid colloidal systems, such as β-LG amyloid fibrils [22,46] and cellulose nanofibrils [47,48]. In the thermodynamically unstable region, the system produces a liquid crystal structure through spinodal decomposition. Both mechanisms lead to the formation of liquid crystal tactoids, whose morphology and internal

arrangement are controlled by the coupled effects of surface tension, osmotic pressure differences, and Frank–Oseen elastic properties [23].

The phenomenon originates from a competition between entropic and enthalpic driving forces. In LLPS, demixing occurs when attractive interactions between macromolecules overcome the entropic gain of mixing. In contrast, LLCPS introduces an additional contribution from shape anisotropy, which favors orientational alignment at high concentrations to minimize excluded volume interactions. The theoretical foundation for such behavior can be traced to Onsager's theory (1949) for the isotropic–nematic transition in suspensions of hard rods [44]. When combined with Flory–Huggins mean-field thermodynamics, which describes concentration-dependent phase separation, the resulting hybrid framework successfully predicts two coupled order parameters—concentration and orientational order—leading to LLCPS.

2.3. Effect of Temperature, pH Value and Ionic Strength on Protein Phase Separation

Proteins can undergo rapid phase transitions with temperature changes. Based on different temperature response mechanisms, protein phase separation can be mainly divided into two categories: (1) When the temperature increases, hydrophobic interactions strengthen, and some protein molecules may aggregate, resulting in lower critical solution temperature type phase separation. (2) When the temperature decreases, hydrogen bonding and electrostatic interactions become dominant, potentially promoting upper critical solution temperature type phase separation. This is an important mechanism for cells to against rapid temperature changes [49]. For example, temperature influences the LLPS of intrinsically disordered proteins by modulating solvent-mediated amino acid interactions. Depending on the sequence-specific balance of hydrophobic and polar residues, proteins can display either upper or lower critical solution temperatures. By incorporating amino-acid-specific temperature-dependent hydrophobicity into coarse-grained models, researchers can more accurately capture these thermos-responsive behaviors [50].

The pH environment is a crucial factor regulating the LLPS process of proteins. Studies have shown that slight pH changes are sufficient to alter the charge state, solubility properties, and intermolecular interactions of biomolecules, thereby affecting their phase separation behavior [51]. Specifically, pH changes alter the protonation degree of certain amino acid residues—such as glutamic acid, aspartic acid, histidine, and lysine—and thus regulate electrostatic interactions and hydrophobic effects between proteins. Under increasingly acidic conditions, residues are more easily protonated, electrostatic repulsion weakens, and attraction strengthens, which often promote the formation of protein aggregates. On the other hand, pH changes also regulate phase separation by altering protein solubility. When the ambient pH is close to the isoelectric point (pI), its net charge tends to be minimal, electrostatic repulsion decreases [52,53]. For example, the microtubule-associated protein Tau exhibits a significant tendency for phase separation near its pI [54]; α-synuclein not only undergoes phase separation more easily under acidic conditions but may also gradually transform into quasi-solid aggregates.

Ionic strength plays a crucial role in regulating protein LLPS, permeating almost the entire process from interaction mechanisms to phase behavior transitions. In low-salt environments, long-range electrostatic attraction between protein molecules is often the core force driving droplet formation. Residues with opposite charges interact through multivalent charge pairing, prompting spontaneous aggregation into liquid condensates. However, as ionic strength gradually increases, salt ions in the solution effectively shield these charge interactions, weakening the Coulomb attraction between molecules, leading to droplet dissolution or dissipation. The study by Lin et al. [55] clearly demonstrates this salt inhibition effect—as NaCl concentration increases, the formation of protein condensates is significantly suppressed,

indicating that electrostatic shielding is an important factor regulating LLPS stability. However, Krainer et al. [56] further discovered that at higher salt concentrations systems exhibited an anomalous phase behavior, and droplets dissolved under medium salt conditions but reappeared in high salt environments. This phenomenon signifies a fundamental shift in the dominant mechanism of phase separation—from electrostatic driving to hydrophobic and nonionic interactions. In other words, when electrostatic attraction is shielded, interactions between hydrophobic residues, π–π stacking, and van der Waals forces gradually become dominant, thereby re-driving the formation of protein condensates.

2.4. Evaporation-Induced Liquid–Liquid Phase Separation

Evaporation not only plays a dominant role in shaping the flow and deposition patterns within droplets, but it is also a typical non-equilibrium environment (NES) that can trigger liquid–liquid phase separation. Guo et al. (2021) [57] observed an evaporation-induced non-associating phase separation phenomenon in a PEG/dextran system. With the spatially uneven distribution of the evaporation flux, the local solute concentration gradually increases. When it exceeds the double-node curve (See Figure 2), the system begins to phase separate, forming dextran-rich microcompartments. These microcompartments not only effectively enrich nucleic acids but also exhibit enhanced ribozyme activity, making them a compelling model for explaining prebiotic compartmentalization. It is worth mentioning that the study demonstrated various phase separation morphologies formed by droplets driven by evaporation under different initial concentrations of PEG and Dextran (as shown in Figure 2b,d).

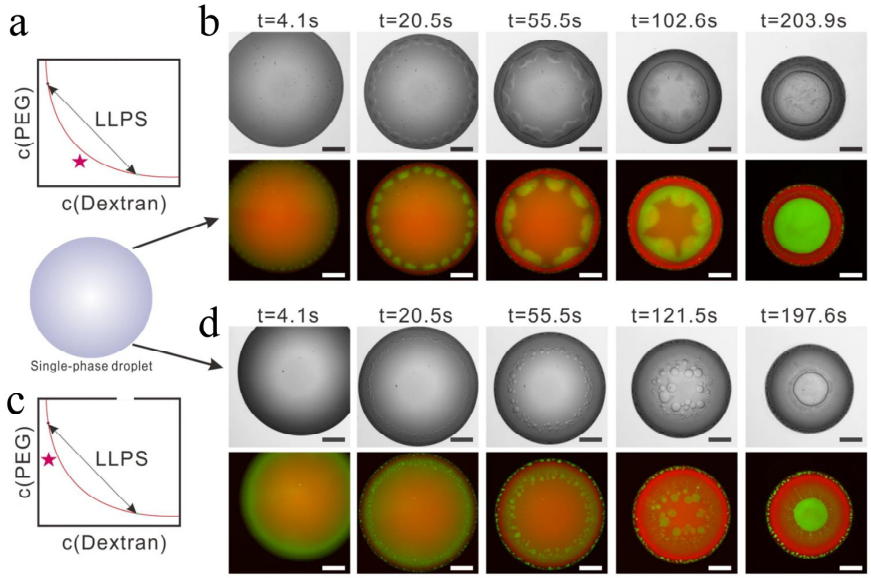

Figure 2. Sequence diagram of phase separation evolution over time during droplet evaporation. (**a**–**c**) Phase diagram of a mixture of PEG and dextran. The solid red line is the binodal line separating the single-phase region from the two-phase coexistence region. The arrow indicates the ATPS junction line, along which the mixture undergoes liquid–liquid phase separation (LLPS) to form a PEG-rich phase and a dextran-rich phase. The positions of the asterisks indicate the concentration dependence of PEG and glucose; a contained 5 wt% PEG–10 wt% dextran, and c contained 9 wt% PEG–4 wt% dextran. (**b**) Evolution of the phase separation pattern within an evaporating droplet, shown in brightfield and fluorescence image sequences, respectively; the dextran-rich phase is labeled with fluorescein isothiocyanate-dextran (FITC-dextran, green), and the PEG-rich phase is labeled with rhodamine B (red). (**d**) Evolution of the phase separation pattern within an evaporating droplet, shown in brightfield and fluorescence image sequences, respectively. The fluorescent labels are the same as in (**b**). For (**b**,**d**), the images were acquired from analysis of seven independent experiments at relative humidity levels ranging from 55% to 65%. The scale bar shows 500 μm [57].

Basically, drying of binary sessile droplets were extensively reported. During the process of evaporation (ethanol and octamethyltrisiloxane), the droplets undergo LLPS, resulting in the appearance of microdroplets at the liquid–air interface [58]. By using high-speed ellipsometry method, Chao et al. revealed that liquid–liquid phase separation may cause active spreading, beyond capillarity or gravity-based laws in the binary mixtures of water and di(propylene glycol) propyl ether. The motion precedes bulk coarsening and is associated with premature interfacial nucleation, due to evaporative enrichment and surface forces [59].

3. LLCPS Behavior of Amyloid Fibril Droplets and the Dynamics of Tactoids

In evaporation-driven protein fibril droplets, solvent evaporation gradually increases the internal protein concentration, causing different regions of the droplet to traverse distinct thermodynamic states at varying rates. This process drives the system into the regime of anisotropic phase formation and induces liquid–liquid crystal phase separation (LLCPS), resulting in the emergence of liquid-crystalline tactoids. When LLCPS occurs through nucleation and growth or spinodal decomposition during the evaporation process, tactoids with different structures are formed [20,22,23]. These structures are the result of self-assembly of protein fibrils under the coupling of limited volume, non-uniform evaporation and interfacial tension.

3.1. Amyloid Fibrils

Amyloid fibrils are anisotropic protein-based colloids that form by self-assembly of aggregates of β-sheets into twisted or helical ribbons in Figure 3a. The fibrillar state of proteins was first discovered in certain diseases and is associated with a variety of protein misfolding, including systemic amyloidosis and many increasingly prevalent neurodegenerative diseases such as Alzheimer's disease and Parkinson's disease [1,2]. Researchers have devoted decades to elucidating their structural characteristics and aggregation dynamic as they are associated with disease. Accumulating evidence suggests that the transformation of proteins into amyloid structures follows a classic nucleation-growth mechanism directly, as exhibited in Figure 3b. In the initial primary nucleation stage, dispersed monomeric proteins interact under specific conditions (such as acidic pH, high temperature, shear, or agitation) to form oligomers. These oligomers slowly self-assemble into a highly ordered primary nucleus, the starting point for fibril growth. Once the primary nucleus is formed, protein monomers rapidly bind to its ends, extending along the fibril axis. Oligomers and short fibril seeds, broken from the elongated fibrils, serve as templates for the addition of monomers and other oligomers to form new fibrils. Simultaneously, the surfaces of large fibril seeds promote branching of existing fibrils, known as secondary nucleation. This nonlinear process significantly accelerates the aggregation rate and leads to the parallel growth of multi-fibril structures [49]. When the system reaches its final thermodynamically stable state, mature amyloid fibrils are formed.

3.2. Temperature Dependence of Amyloid Fibril Formation

The formation process of amyloid fibrils is significantly temperature dependent. Kusumoto et al. (1998) [60] systematically studied the fibrillization kinetics of Aβ protein at 4–40 °C and found that the fibril extension rate constant increased by approximately two orders of magnitude with increasing temperature and conformed to the Arrhenius relationship (activation energy approximately 23 kcal mol^{-1}), indicating that fibril extension involves a significant conformational rearrangement energy barrier. Knowles et al. (2007) [61] further quantitatively measured the thermodynamic parameters of insulin amyloid formation using quartz crystal microbalance technology and found that fibril

extension exhibited significant temperature dependence, with an activation enthalpy of approximately 24 kcal mol^{-1} and a free energy barrier of approximately 6 kcal mol^{-1}. This indicates that the process is enthalpically unfavorable but entropically favorable, representing a typical enthalpy-limited, entropy-driven reaction. Wetzel (2006) [62] pointed out that protein aggregation typically occurs efficiently only when the native conformation is partially destabilized. Therefore, moderate temperature increases can promote the formation of aggregation precursors and accelerate nucleation, while excessively high temperatures may lead to complete protein denaturation, inhibiting the formation of ordered β-sheets. In summary, temperature determines the kinetics and thermodynamic behavior of amyloid fibril formation by regulating the protein conformational energy barrier and the rate of molecular rearrangement.

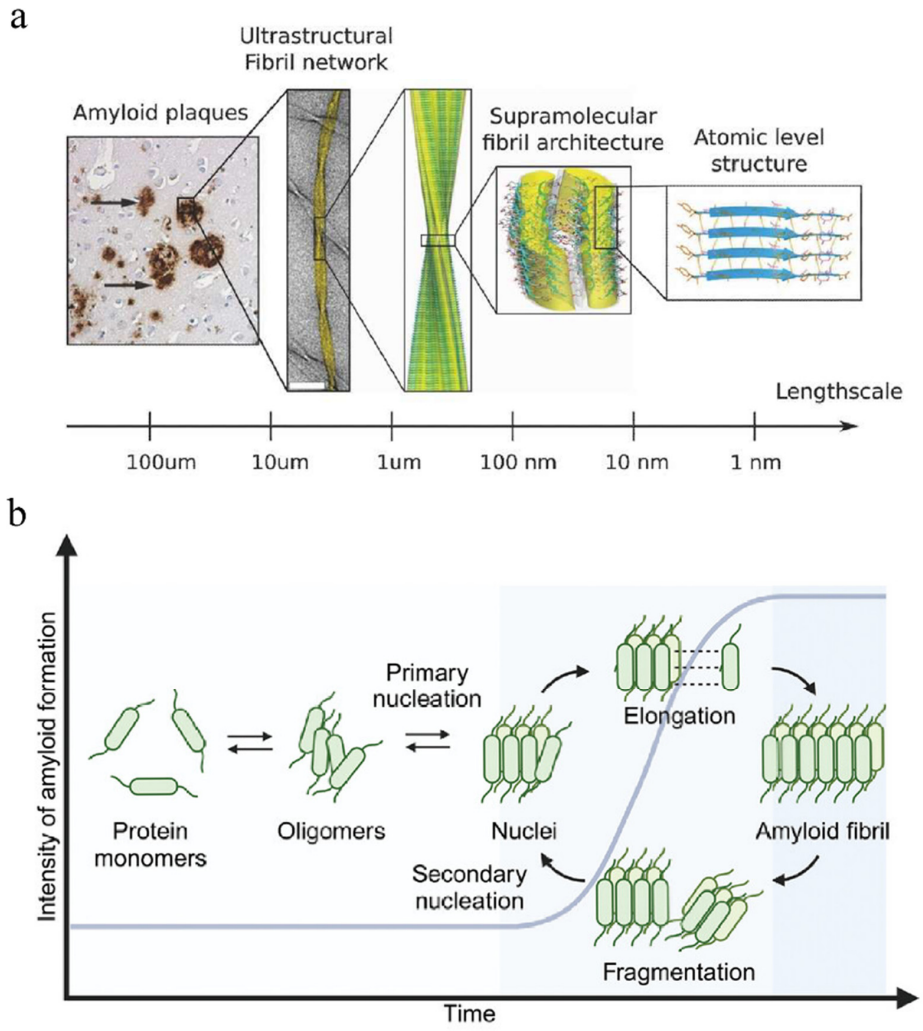

Figure 3. Amyloid fibril structure and protein nucleation phase transition process. (**a**) Different length scales in which amyloid fibrillary structural fingerprints appear. (**b**) Schematic diagram of the amyloid fibrillary formation process through classical nucleation theory. Positive arrows (→): indicate sequential progress (e.g., monomer → oligomer → nucleus → extension → fiber). Bending/feedback arrows (↺): represent key mechanisms such as secondary nucleation (forming new nuclei on existing fibers) and fragmentation (fiber breakage generates new extension sites) [1,49].

3.3. Types and Formation Conditions of Tactoids

During the evaporation of a droplet, due to the high evaporation rate at the edge, the solution concentration first rises near the contact line, which allows it to enter a metastable state (phase separation occurs through nucleation-growth) and an unstable state (phase

separation occurs through spinodal decomposition), thereby producing tactoids. In actual observations, the phase separation produced by spinodal decomposition is often accompanied by radially arranged extended stripes, while nucleation-growth is often accompanied by the gradual growth of isolated tactoids (Figure 4a) [22,23].

Tactoids are equilibrium structures formed during the microscopic phase separation of anisotropic colloidal liquid crystals. Their morphology, internal orientation field structure, and volume are closely related. Based on the classic Frank-Oseen elasticity theory [63] and experimental observations (see in Figure 4b,c), tactoids are mainly divided into three categories: the homogeneous tactoids (where the orientation of the orientation field aligns with the long axis), which are generally smaller and occur during the initial nucleation phase. The bipolar tactoids: the internal pointing vector field of the tactoid changes from uniform to curved along the interface; the cholesteric tactoids: when the tactoid reaches a certain critical volume, the pointing vector field forms a spiral arrangement, and the shape tends to be spherical, which is the tactoid with the largest volume and the highest order parameter. The formation of tactoid is closely related to the length, concentration and volume of protein fibrils: the longer the protofibrils, the more likely the tactoid formed is to present a nematic state (homogeneous or bipolar). Only by shortening the fibril length (<600 nm) can a cholesteric tactoid be formed. This is because shorter fibrils reduce the elastic energy barrier, making it easier for the system to transition to a helical state. Figure 4c demonstrate that the larger the volume of the tactoid, the smaller its aspect ratio, and the structure transitions from a slender state to a nearly spherical state [46,64].

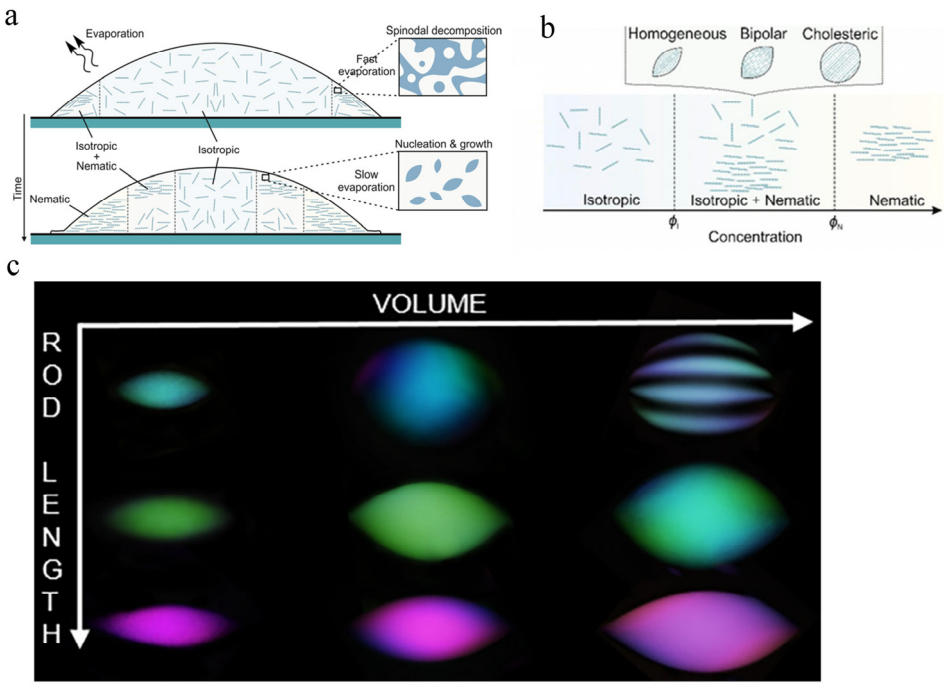

Figure 4. Wetting and drying dynamics of a liquid crystal colloidal droplet on a glass substrate. (**a**) Liquid–liquid crystal phase separation in an anisotropic colloidal drying droplet. (**b**) Liquid crystal phase with rod-like structural units. When the concentration is $\leq \varphi_I$ and $\geq \varphi_N$, the solution is in the isotropic and nematic phases, respectively. Between φ_I and φ_N, the isotropic and nematic phases coexist, and the system undergoes LLCPS, forming different types of crystal aggregates. Upon further evaporation, the volume of the nematic phase increases and the isotropic phase decreases, until the solution becomes completely nematic at φ_N. (**c**) Classification of different haptic types, with the top row (from left to right) showing isotropic, bipolar, and cholesteric, the colors in the image are pseudo-colors used to represent the distribution of liquid crystal phases; the color gradient reflects volume changes or rod length differences [22,64].

3.4. Dynamic Evolution and Sedimentation Patterns of Tactoids

The tactoids formed during droplet evaporation are not static but are driven by the internal flow field, undergoing dynamic migration and evolution (Figure 5). According to research by Yunker et al., for colloids with an aspect ratio of approximately 100, the coffee ring effect is reduced due to colloid aggregation and aggregation. However, for protein fibril solutions, the tactoids formed by evaporating droplets have an aspect ratio of approximately 100. These ellipsoidal, contact-like droplets experience strong capillary interactions, forming a loose stacking or retention structure at the air–water interface, preventing the fibrils from migrating to the edge of the droplet, thereby suppressing the coffee ring effect [22,65].

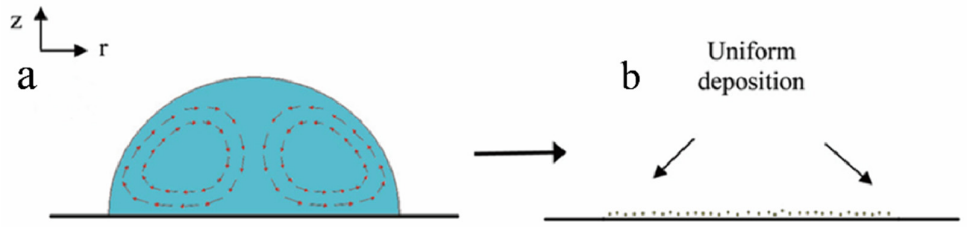

Figure 5. Flow field within a droplet during evaporation. (**a**) Marangoni flow. (**b**) As the evaporation rate slows down, the capillary flow slows, and the competition between capillary and Marangoni flows intensifies. The higher surface tension at the top of the droplet generates Marangoni forces from the contact line to the droplet top. These forces induce flow from the contact line to the droplet top, resulting in the circulatory flow pattern. The recirculating flow evens out the particle concentration, overcoming the formation of coffee stains and leading to uniform deposition, in Figure (**a**), the red dashed arrows indicate the flow path (or diffusion direction) of the fluid on the surface of the hemispherical structure; the black arrows indicate the causal relationship from the flow pattern to the deposition result. In Figure (**b**), the downward arrows indicate the deposition direction, corresponding to the formation of a homogeneous deposition layer. [35].

Furthermore, during the evaporation of the droplet, the experiment observed that the contact line radius of the droplet gradually decreases during the evaporation process. The pinning of the contact line is a prerequisite for the formation of the coffee ring, so the coffee ring effect can be ignored. In the early stage, the tactoid will move radially toward the contact line. This is caused the Marangoni flow [66] caused by the dominant temperature gradient. Since the edge of the droplet evaporates quickly and the temperature is low, the surface tension is large, while the surface tension is low at the center of the droplet (where the temperature is the highest), which pushes the fluid outward [67]. After the droplet shrinks to half its initial radius, the direction of motion reverses, moving toward the center of the droplet. This is likely due to the dominant concentration gradient, which leads to a Marangoni flow, resulting in lower surface tension near the contact line, pushing the fluid inward [68]. In the later stages of droplet evaporation, the tactoid's mobility gradually weakens due to the congestion of the surrounding environment, spatial limitations, and mutual aggregation, and it eventually deposits on the substrate surface.

4. Factors Affecting Proteins/Fibril Deposition

The deposition pattern formed by evaporation-driven protein fibril droplets is affected by a variety of internal and external factors, including evaporation rate [69,70], protein concentration [22,64], surface tension gradient [35], substrate properties [31,71,72] and so on.

4.1. Effect of Evaporation Rate on Deposition Pattern

The evaporation rate directly determines the solute concentration in the droplet and the strength of the internal flow field, which significantly affects the spatial distribution

of the deposition pattern. In the droplet evaporation mode across the contact area, the faster the evaporation rate, the stronger the capillary flow, and more solute particles are transported to the contact line under the action of the internal flow field and aggregated, forming a clear single ring-shaped deposition structure. When the evaporation rate slows down, the capillary flow slows down, and the competition effect between the capillary flow and the Marangoni flow strengthens, the particles are more likely to form multi-point aggregation inside the droplets, producing multiple rings, central aggregation or uniform disk structures [35]. In addition, in the protein fibril droplet system, a lower evaporation rate helps the LLCPS to proceed fully, and the tactoid formation is more stable and orderly; while rapid evaporation may cause the tactoid to not have time to grow and fuse, forming a fragmented or unevenly distributed deposition state [22].

4.2. Role of Concentration

The concentration of the solution is a key parameter that determines whether LLCPS occurs during the evaporation of the droplet. At low concentrations, the volume fraction of the protein fibrils in the system is insufficient to drive the formation of anisotropic phases, resulting in a primarily isotropic, disordered distribution within the droplet [64]. As the concentration of protein fibrils increases, when the critical concentration is reached, the amyloid fibrils will undergo a liquid crystal phase transition, and phase separation from the isotropic phase to the nematic phase will begin to appear inside the droplet, thereby generating isotropic phase + nematic phase domains. These regions usually appear as ellipsoidal tactoid structures with regular birefringence. According to the research of Yunker et al. [65]. The aspect ratio of the resulting tactoids results in significant capillary interactions between them, particularly near the air-water interface, where they spontaneously align and prevent suspended fibrils from reaching the edge of the droplet, thereby suppressing the coffee ring effect. Simultaneously, as the phase-separated region expands, the number of liquid crystal structures (tactoids) increases and attracts and aggregates, causing the originally disordered deposition pattern to evolve during deposition, forming striped or network structures with distinct anisotropic alignment. These structures are not only highly ordered but also exhibit clear directional characteristics.

4.3. Effect of Surface Tension on Deposition Pattern

Surface tension plays a central role in governing how LLPS-derived protein droplets interact with solid interfaces and, consequently, how proteins and fibrils deposit during drying [73–75]. The relatively low surface tension of biomolecular condensates promotes droplet spreading on hydrophilic substrates, increases the contact area, and enhances protein adsorption at the air–water and solid–liquid interfaces. This often results in surface-enrichment and peripheral accumulation of proteins, which, under capillary-driven outward flow during evaporation, leads to ring-like coffee-ring deposition patterns. In contrast, when surface tension is modulated—through substrate chemistry, additives, or environmental conditions—droplet wetting, interfacial enrichment, and subsequent deposition can be significantly altered, influencing fibrillation, nucleation, and the spatial distribution of biomolecules.

Surface tension gradients further dictate deposition through Marangoni flows, which compete with capillary flows inside the droplet. A strong surface tension gradient induces inward Marangoni circulation, suppressing edge deposition and yielding uniform or centrally enriched patterns, whereas a weak or absent gradient allows capillary flow to dominate, concentrating proteins and fibrils at the contact line and forming dense fibrous crusts. These coupled effects of surface tension and its gradients are critical for understanding how LLPS droplets deposit and transform on surfaces, offering strategies to

control condensate patterning, replicate biologically relevant interfacial environments, and regulate surface-mediated fibril formation in vitro.

4.4. Influence of Substrates on Deposition Patterns

During the evaporation process of protein fibril droplets, the physicochemical properties of the substrate are key factors in controlling the final deposition pattern [69,72,76]. Droplets exhibit significant differences in wetting behavior, contact line stability, and interfacial adsorption characteristics on different substrate types. These differences directly influence the evaporation dynamics and solute migration pathways, thereby determining the formation of the deposition pattern.

Substrate wettability has a direct impact on the droplet evaporation pattern. On hydrophilic surfaces (such as glass or silica), droplets typically exhibit a constant contact line mode of evaporation (CCR), where the contact line remains fixed, and the droplet height gradually decreases as it evaporates. In this mode, continuous capillary compensation flow continuously transports solutes near the contact line, easily forming the typical coffee ring [24] deposition structure. On hydrophobic or superhydrophobic surfaces, droplets are more likely to transition from a constant contact line mode (CCR) to a constant contact angle mode (CCA), thereby altering the solute transport pathway and leading to a shift in the deposition structure toward a center-enriched or multi-ring distribution [36].

Recent studies have shown that substrate wettability can have a more profound impact on complex phase separation processes by regulating the internal flow field. Qi et al. [77] revealed that on a hydrophobic substrate wetted by an organic phase, the flow stagnation point formed when a droplet evaporates is the key to maintaining the non-equilibrium phase separation structure. This stagnation point originates from the convective capillary flow induced by the maximum evaporation flux at the liquid–liquid-gas three-phase contact line. It effectively prevents the core-shell microcompartments generated by phase separation from merging and coarsening, allowing them to exist stably as discrete, cell-sized structures (see in Figure 6a). This explains why complex multi-level compartmental structures are maintained on hydrophobic substrates, rather than merging into an equilibrium overall phase separation structure as on clean hydrophilic substrates (in Figure 6b).

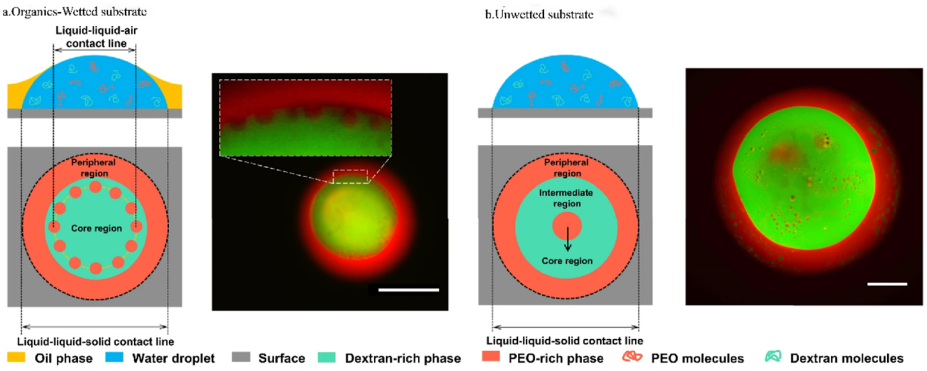

Figure 6. Morphology of an evaporating ATPS droplet resulting from segregative LLPS between PEO and dextran. (**a**) On a hydrophobic substrate moistened with an organic phase, PEO/dextran (protein-free) droplets evaporate to form a ring of dense, cell-sized satellite droplets that do not fuse or migrate and are stably arranged at the edge of the core area. (**b**) On a clean hydrophilic substrate, the same droplet evaporates to form a multi-layer concentric structure in equilibrium without discrete satellite droplets. The dextran- and PEO-rich phases in a-b were labeled with fluorescein isothiocyanate-dextran (FITC-dextran, green) and rhodamine B-polyethylene glycol (rhodamine B-PEG, red). All scale bars are 200 μm [77].

In addition, the wettability of the substrate and the affinity between biomolecules also jointly determine the macroscopic morphology of phase separation. In the presence or absence of protein in the same polysaccharide-protein system, the spatial distribution of the phases after phase separation is completely reversed because the protein changes the affinity between the glucan phase and the substrate [77]. This shows that the interfacial interaction between biomolecules and the substrate is an important factor that must be considered when predicting and controlling the deposition pattern.

For the amyloid fibril system, its deposition pattern is also profoundly regulated by the wettability of the substrate. The surface charge, hydrophobic segments, and tactoid structures of protein fibrils themselves produce specific interactions with the substrate. On hydrophobic surfaces, protein fibrils are more likely to adsorb at the air–liquid interface and form a network structure, which helps to suppress the coffee ring effect and promote uniform deposition. Guo et al. [57] also observed in a non-associative phase separation system that Marangoni flow transports the phase-separated compartments inward rather than forming coffee rings, which also deviates from the typical behavior on hydrophilic substrates. Therefore, precise control of substrate wettability, combined with the interfacial behavior of the protein itself, provides a powerful strategy for achieving precise control of a variety of amyloid protein fibril deposition patterns, from simple coffee rings to complex multi-level compartments.

Furthermore, the surface micro-nanostructure and chemical functionalization often influence the direction of the deposition pattern. For example, roughness at the micro-nanoscale can make the contact line less likely to slide; combined with some directional wettability design, the droplet may be forced to evaporate in an asymmetric manner, resulting in striped, star-shaped, or mesh-like deposition patterns [78]. Meanwhile, if functional groups—such as carboxyl, amino, or even PEG—are added to the surface through chemical modification, the affinity between the protein molecules and the interface can be altered, thereby regulating the migration path and arrangement of the fibrils within the droplet. PEG modification, in particular, has been widely used in the field of anti-biofouling, significantly improving the consistency and stability of the deposited structure in applications such as protein deposition, electrowetting manipulation, or micro-area patterning [79–81]. Overall, the physical and chemical properties of the substrate largely determine the final morphology of the protein deposition pattern by regulating evaporation kinetics, interfacial adsorption, and internal flow. Targeted design of substrate surface properties not only helps us understand the underlying mechanisms of biomacromolecule self-assembly but also provides a viable strategy for constructing controlled deposition patterns and developing novel bio-functional interfaces.

5. Strategies for Regulating Protein Droplet Deposition Patterns

As discussed above, the final deposition pattern formed by a droplet during evaporation depends not only on its internal structure and flow behavior, but also on the forces acting on the particles. To precisely control the deposition pattern of protein fibril droplets, various external interventions are used to modulate the internal flow, interfacial behavior, and protein aggregation orientation of the droplets, thereby shaping deposition patterns with specific morphologies and functions. Current strategies include external field-directed orientation control [29,82–85], substrate geometry constraints [28,86,87], and surface functionalization [30,88,89].

5.1. External Field Control of Deposition Mode

The formation and arrangement of liquid crystal structures, such as tactoids, during evaporation can be conceptualized within the framework of external field control. The

inherent properties of protein fibrils, such as their rigid backbone [90], anisotropy [91], and responsiveness when interacting with interfaces [92], make their self-assembly process somewhat similar to the behavior of liquid crystal colloids or rod-shaped nanoparticles under external fields. Therefore, in the following sections, we discussed several common control methods in protein droplet systems.

In anisotropic nanoparticles and liquid crystal molecules, an external AC electric field can drive the particles to arrange head-to-tail by inducing dipole moments, forming a long-range ordered structure [93]. Analogously, rod-like fibrils within a protein droplet can also deform the overall droplet morphology and change the orientation of the tactoids under the influence of an electric field. Previous studies have shown that electric fields can enhance the molecular orientation and orientation field at the edge of a protein droplet, potentially driving the transition of the deposition pattern from a diffuse to a ribbon-like arrangement (e.g., the formation of fibril clusters under the influence of the double electric layer) [29]. Furthermore, the frequency and intensity of the electric field can be used to adjust the aspect ratio and distribution density of the tactoids, thereby achieving fine control over the phase behavior inside the droplet. This method provides the possibility of constructing directionally responsive protein deposition patterns.

The role of the light field, especially the focused laser beam, is not only to input energy, but also to manipulate the spatial arrangement of molecules. In 2024, Zhang et al. reported an interesting strategy: they used femtosecond laser direct writing technology to achieve the programmable arrangement of liquid crystal molecules without an additional external field [82]. In this method, the scanning path, power and scanning speed of the laser are key parameters. By adjusting these conditions, the liquid crystal precursor molecules will be neatly arranged along the laser direction under the combined action of the light field gradient and the local shear flow, and will polymerize and solidify almost synchronously, leaving behind a highly ordered three-dimensional structure. The core here is not the common electric or magnetic field drive, but the anisotropic orientation brought about by shear induction [94–96]. This provides a new avenue for the manipulation of protein fibril droplets. By analogy, if a droplet is placed under a controlled laser scanning path and superimposed with a shear field caused by rapid local evaporation, it is possible to make the tactoids of the protein fibril more ordered, resulting in a deposition pattern with a sense of direction and structure. This approach is not only highly spatially selective but also highly flexible, making it ideal for processing protein materials into multifunctional micro-structured devices.

For colloidal systems containing paramagnetic nanoparticles, an external magnetic field can induce magnetic dipole effects, driving the particles to self-assemble into chain, ribbon, or even network structures in the direction of the magnetic field [83,84]. A similar mechanism can be exploited by integrating magnetically responsive materials into protein fibril systems. For example, by combining magnetic nanoparticles with protein fibrils, magnetic fields can be used to manipulate the alignment of tactoids and even induce anisotropic stretching of the droplet boundary. This magnetic field responsiveness holds great value in applications such as biofunctional interfaces and dynamic sensors [97–99].

5.2. Effect of Substrate Microstructure and Geometric Template

The surface morphology and chemical functionality of the substrate are also key factors influencing the deposition behavior of protein droplets. Micro- and nano-patterning techniques, such as photolithography and microcontact printing, can be used to create arrays of grooves, protrusions, or selectively wetted areas on the substrate. This can restrict contact line movement, generate localized differences in evaporation flux distribution, and

trigger capillary flow reconstruction, significantly affecting the deposition orientation and macroscopic pattern of protein fibrils [28,100].

Park et al. (2021) [31] designed a spatial confinement system with a microchannel structure. By using the stick-slip behavior of the contact line during droplet evaporation, the droplet undergoes periodic decoupling and reattachment at the edge of the micro-structured groove during the process, inducing the deposition of protein fibrils at specific locations at the edge of the channel, thereby guiding the deposition of protein fibrils along the long axis of the groove, forming a periodic, regularly arranged fibril ribbon structure (Figure 7a–d). The study found that the width of the microchannel determines the arrangement spacing between fibrils, while the interfacial curvature of the groove sidewall affects the location and direction of local concentration and liquid crystal phase transition. Tactoids migrate under the action of the flow field and are captured at the edge of the channel, thereby achieving the orderly deposition of anisotropic patterns on a macro scale. This method is suitable for constructing soft material patterns with optical and mechanical functional gradients.

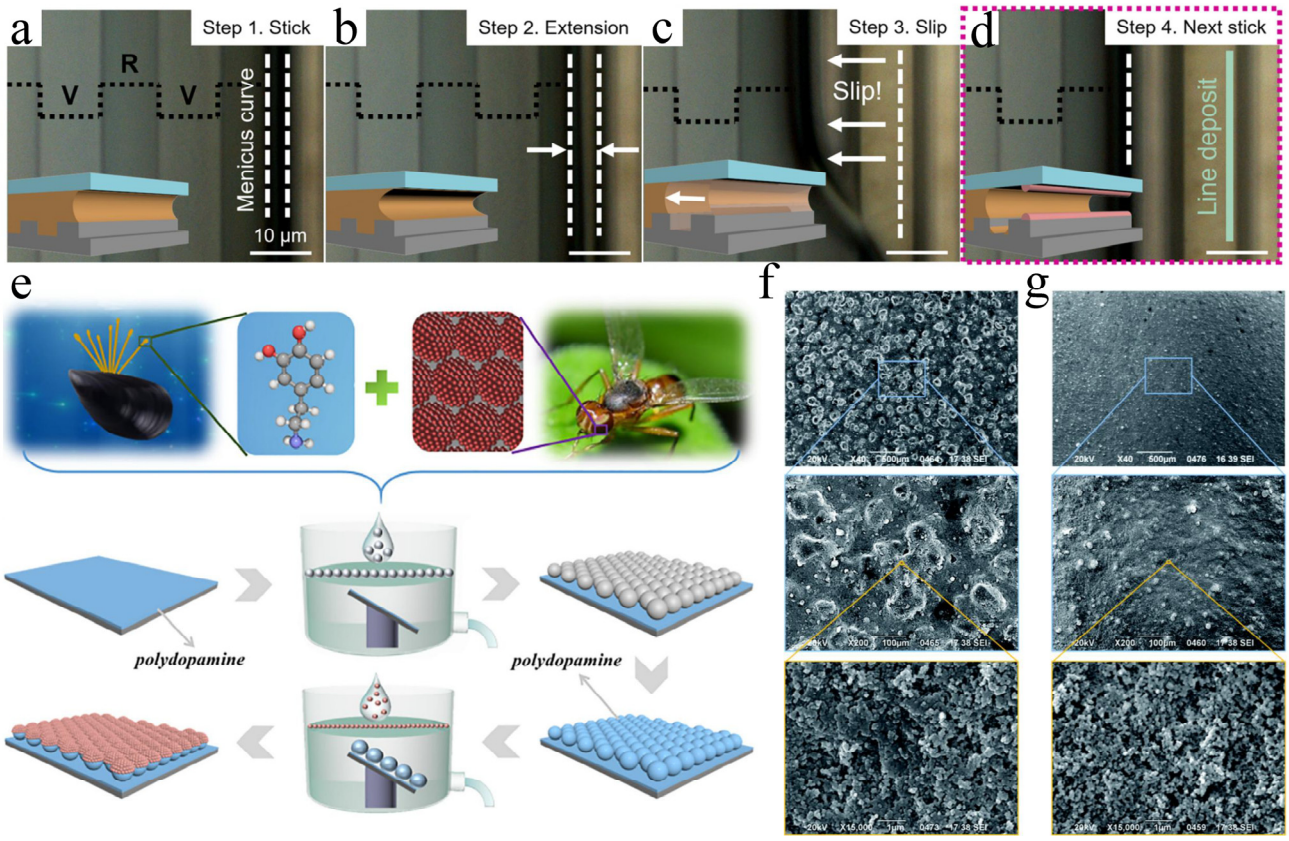

Figure 7. Microstructures and geometric templates of some substrates. (**a**–**d**) Real-time observation of the drying process using an optical microscope (ZEISS, Oberkochen, Germany). The contact line of the solution exhibits stick-slip motion on the ridges and valleys of the channel, in (**a**–**d**), V refers to the groove (represented as valley) of the substrate microstructure, while R represents the protrusion (also known as the ridge of the channel), and the white arrows indicate the sliding direction of the solution contact line. (**e**) A hierarchical membrane with superhydrophobic properties, inspired by the superstrong adhesion of mussels and the hierarchical structure of mosquito compound eyes. (**f**,**g**) SEM micrographs of BTNW (**f**) and TNW (**g**) surfaces at different magnifications (increasing from top to bottom) [31,86,89].

Zhang et al. (2020) [86] used SiO_2 nanoparticles and polystyrene microspheres of different sizes in their study. The super-hydrophobic surface constructed by liquid–air

interface self-assembly mimicking the structure of insect compound eyes is shown in Figure 7e. This structure has significant anti-adhesion and directional selectivity, which is conducive to the self-cleaning movement and directional contraction of droplets on its surface, providing a new strategy for inducing deposition on complex structure surfaces.

Superhydrophobic material to construct an electrowetting system was also investigated [89] (Figure 7f,g). Experimental measurements showed that the droplet roll-off angle on the top coated nanowire (TNW) surface was much lower than that on Cytop® (Agc Chemicals Americas Inc., Exton, PA, USA). Both TNW and base coated and top coated nanowire (BTNW) surfaces, when used with fluorescently labeled proteins, exhibited a typical micro-nano dual-layer roughness. This structure creates a Cassie–Baxter state, where the droplet is suspended at an air-solid composite interface, significantly reducing the solid–liquid contact area and thus significantly weakening the adhesion between the protein and the substrate. The adsorption capacity was significantly reduced, demonstrating that the superhydrophobic surface effectively inhibits protein adsorption and contamination. Because droplets practically "float" and slide on this low-adhesion surface, they encounter minimal resistance during migration, and the solute distribution inside the droplet is more uniform. Therefore, for protein droplets, superhydrophobic surfaces can significantly weaken their interaction with the substrate, making it easier for droplets to maintain uniform morphology and composition as they migrate and distribute on the surface. When the electric field regulation is superimposed, the electric field can drive and transport the droplets more effectively within the microstructure area, and at the same time, the anti-pollution stability of the entire device in the face of high-concentration protein systems is significantly improved. In other words, this method not only improves the transmission efficiency, but also takes a step forward in practicality. It is especially suitable for complex biological molecular environments that are prone to surface contamination.

5.3. Control of Wetting and Deposition by Surface Functionalization

Surface functionalization is an important means to regulate the deposition pattern of protein fibril droplets. It changes the wettability of the droplets by changing the surface energy, chemical composition and microstructure of the substrate. The change in wettability will affect the internal flow behavior [30,88]. Therefore, the migration path of the solute will change accordingly, thereby changing the final deposition pattern.

Wettability is almost a key factor in determining the behavior of the deposition. The classic Young equation states that the contact angle of a droplet on a solid surface is determined by the energy balance at the solid–gas [101], solid–liquid, and liquid–gas interfaces [102]. However, in experiments, surface modification is often used to manipulate the surface. For example, introducing chemical groups—fluorinated alkyl chains can make the surface very hydrophobic, while carboxyl and amine groups can become more hydrophilic. Furthermore, by applying microstructural modifications, the contact angle can be increased from less than 10° (superhydrophilic) to greater than 150° (superhydrophobic), a wide range [103–105]. For example, plasma copolymerization can be used to deposit acrylic acid with carboxyl groups together with hydrophobic monomers, such as fluorinated hydrocarbons. By adjusting the input power and monomer ratio, a functional layer with an energy gradient can be constructed on the surface, thereby more precisely controlling the contact angle [88]. Another idea is to use the layer-by-layer assembly of polyelectrolyte multilayer membranes, which can regulate the thickness and surface hydrophilicity at the nanoscale. The key is that this method is applicable to various complex surfaces and is not restricted by the shape of the substrate [30].

6. Applications of Droplet Deposition

The deposition patterns formed by protein fibril droplets driven by evaporation are of great significance beyond basic research. These deposition patterns are adjustable and programmable, and the arrangement and orientation of the protein fibrils during the deposition process are also quite orderly. Because of these characteristics, they show great potential in cutting-edge fields such as self-assembled nanostructures, biomedicine and flexible electronics. This type of droplet deposition is not only a model system for understanding self-assembly behavior, but also provides experimental and conceptual support for the design of controllable functional materials [2,14,31,98,106,107].

6.1. Self-Assembled Nanostructure Construction

Protein fibrils possess excellent anisotropy and surface functionalization capabilities. Their cross-beta core structure, perpendicular to the long axis of the fibrils, offers excellent mechanical properties and high tensile strength, making them ideal nanoscale template materials [90,91,108].

Park et al. [31] designed a protein fibril deposition strategy based on micro-structured substrates and geometrically confined templates. They dripped a β-lactoglobulin solution onto a micro-structured template surface with striped grooves and exploited evaporation-induced stick-slip behavior to control the pinning and sliding of contact lines, thereby forming a periodically deposited protein fibril structure between the template grooves. Crucially, the surface of amyloid fibrils is rich in functional groups such as carboxyl, amide, and phenolic hydroxyl groups. These functional groups not only electrostatically adsorb metal ions but also serve as natural reduction sites, promoting the in situ reduction of metal ions to form nanoparticles without the need for external reducing agents [108]. As illustrated in Figure 8a–d, Park et al. exploited this property by modifying the surface of protein fibrils with gold nanoparticles (AuNPs), successfully constructing conductive metal-protein composite microwire arrays. Their conductivity reached ~10^{-3} S/m, comparable to some carbon nanomaterials. This study demonstrates the practical feasibility and engineering potential of protein droplet deposition patterns in the construction of nanowires, microscale circuits, and flexible sensors.

In recent years, the self-assembled deposition patterns formed by droplets driven by evaporation have attracted considerable attention in the field of functional materials construction. Gong et al. reported that when a uniform aqueous dispersion containing polyethylene glycol (PEG) and protein was dropwise added to a glass substrate in the presence of ammonium sulfate [109], a salt layer spontaneously formed at the solid-liquid interface, triggering a secondary LLPS event. This interface-induced LLPS triggered competitive diffusion of the polymer-rich phase, ultimately spontaneously forming a microscale concentric ring deposition pattern (Figure 8e). They successfully extended this mechanism to structurally identical biomacromolecules, such as single-nucleotide variant DNA, which can autonomously partition into concentric rings. This process, through competitive spreading induced by the salt layer formed at the solid-liquid interface, achieved micron-scale concentric ring separation. Furthermore, the salt-dissolution effect enabled the selective extraction of specific DNA sequences with a purity of up to 97% (Figure 8f). This study demonstrates that DLLPS-driven deposition is not only a non-equilibrium self-organizing process but also an effective platform for molecular differentiation and precise spatial patterning.

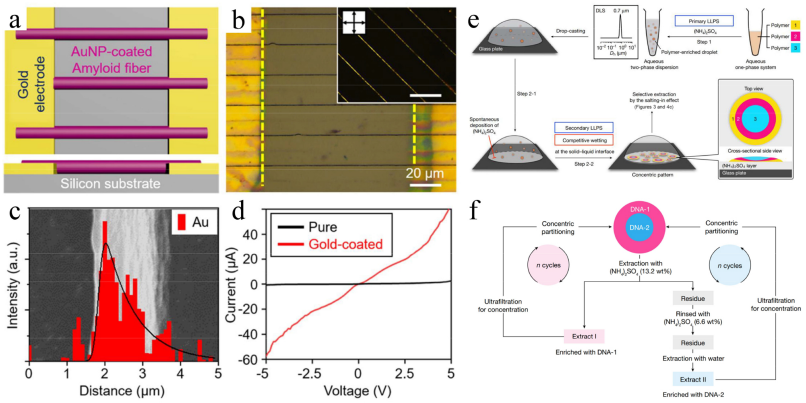

Figure 8. Some applications of amyloid fibril deposition structures in the construction of self-assembled nanostructures. (**a**) Schematic diagram of the structure of an AuNP-coated amyloid wire on a silicon substrate. (**b**) The top image is an OM image of the sample, and the inset is a POM image after the sample was rotated 45°. As before, the amyloid complex exhibits birefringence on the substrate. The white scale bar represents 20 μm, in Figure (**b**), the yellow dashed line marks the location of the AuNP-coated amyloid fibers on the silicon substrate (main image) and indicates the boundary of the birefringent region in the polarizing microscope inset (POM). (**c**) EDX line scan of the gold element on the wire. The graph is plotted along the x-axis of the background SEM image. (**d**) Voltage-current curves of pure and AuNP-coated amyloid wires. (**e**) Schematic of the concept and procedure for the concentric partitioning of nearly identical macromolecules by LLPS followed by competitive surface wetting: A homogeneous mixture of three polymers in water undergoes $(NH_4)_2SO_4$-induced primary LLPS (step 1), affording an aqueous two-phase dispersion, in which polymer-enriched droplets are dispersed in an $(NH_4)_2SO_4$-enriched continuous aqueous phase. When this aqueous two-phase dispersion is subjected to drop-casting onto a glass plate, an $(NH_4)_2SO_4$ layer spontaneously forms on the glass surface (step 2-1), in which the polymer-enriched droplets deposit onto the $(NH_4)_2SO_4$ layer and undergo secondary LLPS at the solid–liquid interface. Finally, the resulting three phases competitively wet the surface of the $(NH_4)_2SO_4$ layer to furnish concentric patterns (step 2-2). Top inset, DLS profile of the aqueous two-phase dispersion. Bottom inset, schematic top view and cross-sectional side view of the concentric pattern. (**f**) Flowchart for selective extraction of DNA from concentrically partitioned mixtures via salting effect [31,109].

6.2. Flexible Electronic and Optoelectronic Functional Materials

Protein fibril droplets induce directional deposited textures during evaporation. These patterns not only play a unique role in microstructural control but are also increasingly recognized as a new approach for flexible electronic and optoelectronic functional materials. Amyloid is considered by many researchers to be a promising functional material due to its inherently highly ordered β-sheet structure, rich surface functional groups, and strong interfacial bonding ability.

Flexible electronic devices derived from this type of protein deposition structure have received increasing attention in recent years. For example, Chen's work tried to combine amyloid protein with polysaccharides (such as sodium alginate) to make a hybrid nanomembrane shown in Figure 9a [14]. It was used as a transition layer for metal deposition. They found that this film could grow a high-strength conductive layer without obvious cracks on a flexible polymer substrate. Under repeated bending or stretching, the metal layer remained resistant to fracture and its conductive properties remained quite stable, performing very well in devices such as flexible OLEDs. Zhang et al. imported functional groups on the surface of protein fibrils as reduction and fixation sites for metal ions (such as silver and gold), allowing these ions to be reduced and self-assembled in situ, providing a green synthesis path to obtain a conductive layer with excellent performance [16]. Han et al. went a step further and introduced the protein membrane into a flexible substrate to create a sandwich sensor structure (Figure 9b,c) [98]. It contains both a protein film modified with magnetic nanoparticles and a

conductive protein film reinforced with carbon nanotubes. This design allows the device to produce reversible microcracks under the action of external force deformation or magnetic field, which in turn causes resistance changes, enabling the detection of strain or magnetic signals. The measured response time is about half a second, indicating that its real-time and repeatability are excellent. Such flexible and stretchable sensors are likely to be integrated into wearable devices in the future, such as for identifying human movements, remote health monitoring, and even in human-computer interaction scenarios. In addition, the directional structure formed by protein deposition itself also suggests their potential use in optoelectronic waveguides, microlens arrays and other fields.

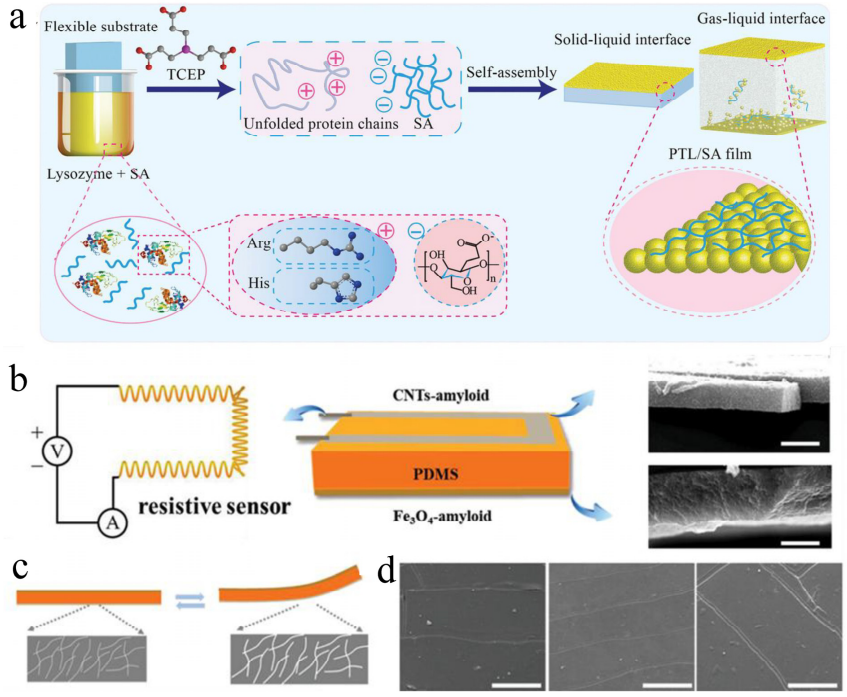

Figure 9. Some applications of amyloid fibril deposition structures in flexible electronic and optoelectronic functional materials. (**a**) Schematic diagram of the basic preparation process of PTL/SA nanofilm coatings, the arrows in Figure (**a**) represent the fabrication process of PTL/SA nanofilms: starting with flexible substrate treatment, proceeding through protein chain unfolding and self-assembly, ultimately forming a film at the gas-liquid and solid-liquid interfaces. The arrow directions indicate the sequence of steps and molecular migration pathways. (**b**) Sandwich structure of a magnetic sensor. SEM image showing a cross-section of the conductive layer (top) and magnetic layer (bottom). The scale bar shows 5 μm. (**c**,**d**) Schematic diagram and SEM images of cracks in the conductive layer under increasing bending conditions. The scale bar shows 200 μm, in Figure (**b**), the arrows indicate the direction of current flow in the sensor circuit; in Figure c, the arrows indicate that tensile stress during bending tests can cause cracks in the conductive layer [14,98].

6.3. Potential Bioapplications

Hybrid membrane was constructed based on β-lactoglobulin amyloid fibrils and ZrO_2 nanoparticles (CAF-Zr) [16]. ZrO_2 nanoparticles (<10 nm) were synthesized through in situ reduction of charged amino acid group templates on the surface of protein fibrils (Figure 10). Then the amyloid fibrils and ZrO_2 nanoparticles were deposited on the activated carbon support layer through vacuum filtration to form a functional membrane structure. The CAF-Zr hybrid membrane exhibits excellent selective removal of fluoride ions, with a removal efficiency of more than 99.5% at a pollutant concentration of up to 200 mg/L. Its ion distribution coefficient (Kd) is as high as 6820 mL/g. The result shows a great potential of protein/inorganic composite structures constructed by droplet deposition in environmental

water treatment and biological separation. Based on the isoelectric point of amyloid protein fibrils and their extremely strong surface activity, Han et al. proposed an electrostatic self-assembly strategy [98]. By introducing phytic acid, a low-molecular-weight but highly charged cohesive protein film are regulated. Furthermore, advanced functional protein films are prepared at the air-liquid interface. The resulting protein films can be applied as functional coatings on a variety of substrates, significantly improving their hydrophilicity and biocompatibility, providing a reliable approach for surface functionalization of biomembranes, tissue engineering scaffolds, and implantable medical devices.

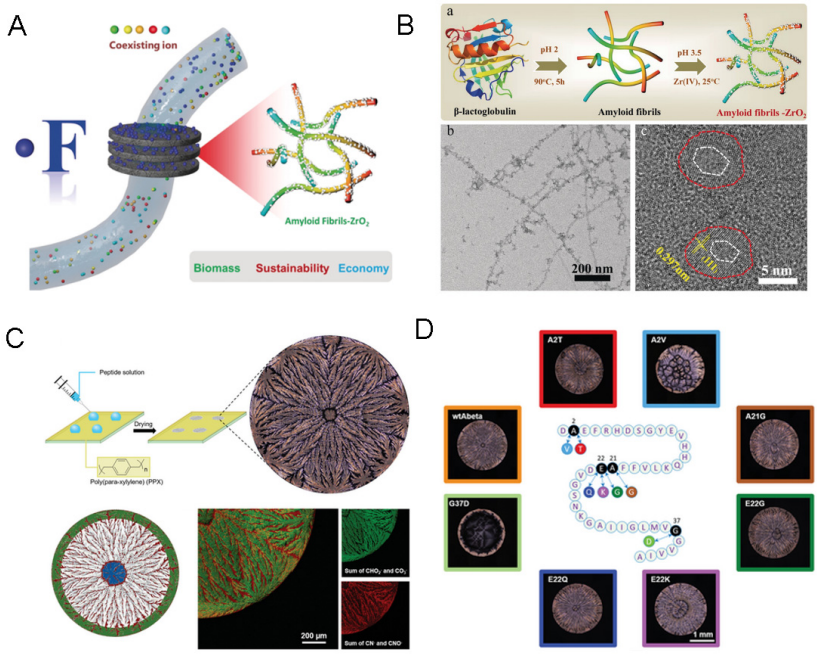

Figure 10. Some biomedical applications of amyloid deposition structures. (**A**) A hybrid membrane based on carbon and amyloid fibril nano-ZrO_2 composites [16]. (**B**) The synthesis of mixed amyloid fibrils-ZrO_2. Figure (**B**) (a) shows the schematic diagram of the synthesis of mixed amyloid fibrils coated with ZrO_2. Arrows in the diagram indicate the sequence of synthesis steps and the switching of reaction conditions: β-lactoglobulin proteins aggregate into amyloid filaments under acidic/high temperature conditions, and then is treated with Zr(IV) solution to form a ZrO_2 coating layer. Figure (**B**) (b) shows the TEM image of amyloid fibrils coated by ZrO_2. Scale bar is 200 nm. Figure (**B**) (c) demonstrates the high-resolution TEM image of amyloid fibrils coated by ZrO_2. White marking indicates the amorphous core of the particles and red marking indicates the outline of the particles having the crystalline structure. Scale bar is 5 nm. (**C**) Peptide stains are obtained by depositing droplets of an aqueous carbonate buffer solution onto hydrophobic poly(para-xylylene) coated glass wafers. A representative polarized light microscopy (PLM) image of the dried stain obtained from Aβ42 reveals complex deposition patterns, chemical analysis of a dried Aβ42 peptide stain using ToF-SIMS imaging: salt crystals, marked in green, are identified by CHO_2^- and CO_3^- fragment ions and the Aβ42 peptide, marked in red, is identified by CN^- and CNO^- fragments. Scale bars are 1, 2, and 5 μm. (**D**) The central schematic diagram shows the amino acid sequence and mutation sites of Aβ42 (arrows indicate single-point mutation locations), surrounded by PLM images of the corresponding mutants; the arrows connect the mutation sites to the experimental results, indicating the impact of mutations on deposition patterns [16,110].

Proteins derive their biological functions from their intricate structures, and even minor conformational changes can trigger pathological aggregation, as seen in amyloid beta (Aβ42) peptides associated with Alzheimer's disease. Traditional methods for studying misfolding, such as NMR or cryo-EM, are complex or limited to late-stage fibril formation. Azam et al. [110] introduces a simple yet powerful alternative: analyzing stain patterns left by drying droplets of Aβ peptides (Figure 10). Using pretrained deep-learning algorithms, the researchers achieved

over 99% accuracy in distinguishing structural variants of Aβ42 from their characteristic deposition patterns. These results reveal that protein-derived stains act as reproducible fingerprints of molecular structure, offering a fast, low-cost tool for probing protein misfolding and potentially enabling early diagnostics of neurodegenerative diseases.

The condensed droplets formed in LLPS possess two core characteristics: selective molecular enrichment capability, enabling the efficient concentration of specific catalysts, substrates, or biomacromolecules within confined droplets [111–113]; excellent microcellular compartmentalization properties, providing a spatially isolated microenvironment for chemical reactions. These characteristics make it highly promising for the construction of biomimetic high-performance microreactors [114–117]. In recent years, researchers have successfully applied LLPS to various biomimetic systems, leveraging its controllability and biocompatibility, such as constructing microreactors with high reaction efficiency [118,119] and developing drug delivery carriers with intelligent response characteristics [120], and designing artificial cell models with energy conversion and signal modulation functions [119]. These studies demonstrate that LLPS is not only an important mechanism for understanding the molecular organization and dynamic regulation within cells but also provides new ideas for the design of novel functional materials and bioengineering systems.

7. Summary

This article examines the self-assembly and deposition patterns of protein/fibril droplets driven by evaporation. Previous research indicates that droplets typically undergo a gradual transition from a relatively uniform liquid distribution to an anisotropic, ordered deposition structure. The mechanisms involved are quite complex, including internal capillary flow, Marangoni effect, phase separation, and the formation and evolution of tactoids. These factors are influenced by the combined effects of evaporation rate, concentration gradient, surface tension, and interfacial conditions, reflecting the unique coupling of rheological and phase behavior characteristics of protein/fibril systems. In recent years, the number of methods for controlling deposition has significantly increased. In addition to the common methods of interfacial electrical assembly and external field actuation, researchers have also explored the use of micro-structured templates and surface modifications to guide droplet deposition trajectories. These methods generally improve directionality and uniformity and even impart new functionalities to the deposited layer. More notably, combining the evaporation process with multi-physics techniques such as laser micro-nanofabrication and magnetic response control has significantly expanded the freedom of pattern construction, making structural design more programmable.

Author Contributions: Conceptualization, D.L.; investigation, X.Z., C.W. and D.L.; writing—original draft preparation, X.Z. and C.W.; writing—review and editing, X.Z., Z.W. and D.L. All authors have read and agreed to the published version of the manuscript.

Funding: This work was supported by the Fundamental Research Funds for the Provincial Universities of Zhejiang, the National Natural Science Foundation of Ningbo (Grant No. 2024J198), Qian Xuesen Collaborative Research Center of Astrochemistry and Space Life Sciences Fund, and K. C. Wong Magna Fund in Ningbo University.

Data Availability Statement: All new data obtained in this work are contained in the tables and graphs presented in the article.

Conflicts of Interest: The authors declare no conflicts of interest.

References

1. Knowles, T.P.J.; Mezzenga, R. Amyloid Fibrils as Building Blocks for Natural and Artificial Functional Materials. *Adv. Mater.* **2016**, *28*, 6546–6561. [CrossRef]

2. Knowles, T.P.J.; Buehler, M.J. Nanomechanics of functional and pathological amyloid materials. *Nat. Nanotechnol.* **2011**, *6*, 469–479. [CrossRef]
3. Ling, S.; Li, C.; Adamcik, J.; Wang, S.; Shao, Z.; Chen, X.; Mezzenga, R. Directed Growth of Silk Nanofibrils on Graphene and Their Hybrid Nanocomposites. *ACS Macro Lett.* **2014**, *3*, 146–152. [CrossRef]
4. Ling, S.; Li, C.; Adamcik, J.; Shao, Z.; Chen, X.; Mezzenga, R. Modulating Materials by Orthogonally Oriented β-Strands: Composites of Amyloid and Silk Fibroin Fibrils. *Adv. Mater.* **2014**, *26*, 4569–4574. [CrossRef]
5. Knowles, T.P.J.; Oppenheim, T.W.; Buell, A.K.; Chirgadze, D.Y.; Welland, M.E. Nanostructured films from hierarchical self-assembly of amyloidogenic proteins. *Nat. Nanotechnol.* **2010**, *5*, 204–207. [CrossRef] [PubMed]
6. Chen, C.; Wu, C.; Yang, T.; Zhao, W.; Lei, J.; Lin, D. Changing the amyloid nucleation process using small molecules and substrates: A way to build two-dimensional materials. *Nanoscale* **2025**, *17*, 5788–5797. [CrossRef]
7. Yang, T.; Yu, T.; Zhao, W.; Lin, D. Tunable inhibition of β-amyloid peptides by fast green molecules. *Chin. Phys. B* **2021**, *30*, 088701. [CrossRef]
8. Reynolds, N.P.; Charnley, M.; Mezzenga, R.; Hartley, P.G. Engineered Lysozyme Amyloid Fibril Networks Support Cellular Growth and Spreading. *Biomacromolecules* **2014**, *15*, 599–608. [CrossRef] [PubMed]
9. Mostaert, A.S.; Higgins, M.J.; Fukuma, T.; Rindi, F.; Jarvis, S.P. Nanoscale Mechanical Characterisation of Amyloid Fibrils Discovered in a Natural Adhesive. *J. Biol. Phys.* **2006**, *32*, 393–401. [CrossRef]
10. Nguyen, P.Q.; Botyanszki, Z.; Tay, P.K.R.; Joshi, N.S. Programmable biofilm-based materials from engineered curli nanofibres. *Nat. Commun.* **2014**, *5*, 4945. [CrossRef]
11. Lin, D.; Lei, J.; Li, S.; Zhou, X.; Wei, G.; Yang, X. Investigation of the Dissociation Mechanism of Single-Walled Carbon Nanotube on Mature Amyloid-beta Fibrils at Single Nanotube Level. *J. Phys. Chem. B* **2020**, *124*, 3459–3468. [CrossRef]
12. Lin, D.; Qi, R.; Li, S.; He, R.; Li, P.; Wei, G.; Yang, X. Interaction Dynamics in Inhibiting the Aggregation of Aβ Peptides by SWCNTs: A Combined Experimental and Coarse-Grained Molecular Dynamic Simulation Study. *ACS Chem. Neurosci.* **2016**, *7*, 1232–1240. [CrossRef] [PubMed]
13. Li, C.; Adamcik, J.; Mezzenga, R. Biodegradable nanocomposites of amyloid fibrils and graphene with shape-memory and enzyme-sensing properties. *Nat. Nanotechnol.* **2012**, *7*, 421–427. [CrossRef]
14. Chen, M.; Yang, F.; Chen, X.; Qin, R.; Pi, H.; Zhou, G.; Yang, P. Crack Suppression in Conductive Film by Amyloid-Like Protein Aggregation toward Flexible Device. *Adv. Mater.* **2021**, *33*, 2104187. [CrossRef]
15. Bolisetty, S.; Vallooran, J.J.; Adamcik, J.; Mezzenga, R. Magnetic-Responsive Hybrids of Fe_3O_4 Nanoparticles with β-Lactoglobulin Amyloid Fibrils and Nanoclusters. *ACS Nano* **2013**, *7*, 6146–6155. [CrossRef] [PubMed]
16. Zhang, Q.; Bolisetty, S.; Cao, Y.; Handschin, S.; Adamcik, J.; Peng, Q.; Mezzenga, R. Selective and Efficient Removal of Fluoride from Water: In Situ Engineered Amyloid Fibril/ZrO_2 Hybrid Membranes. *Angew. Chem. Int. Ed.* **2019**, *58*, 6012–6016. [CrossRef] [PubMed]
17. Li, C.; Qin, R.; Liu, R.; Miao, S.; Yang, P. Functional amyloid materials at surfaces/interfaces. *Biomater. Sci.* **2018**, *6*, 462–472. [CrossRef]
18. Jin, T.; Peydayesh, M.; Li, M.; Yao, Y.; Wu, D.; Mezzenga, R. Functional Coating from Amyloid Superwetting Films. *Adv. Mater.* **2022**, *34*, 2205072. [CrossRef]
19. Lin, D.; Qian, Z.; Bagnani, M.; Hernández-Rodríguez, M.A.; Corredoira-Vázquez, J.; Wei, G.; Carlos, L.D.; Mezzenga, R. Probing the Protein Folding Energy Landscape: Dissociation of Amyloid-β Fibrils by Laser-Induced Plasmonic Heating. *ACS Nano* **2023**, *17*, 9429–9441. [CrossRef]
20. Lin, D.; Bagnani, M.; Almohammadi, H.; Yuan, Y.; Zhao, Y.; Mezzenga, R. Single-Step Control of Liquid–Liquid Crystalline Phase Separation by Depletion Gradients. *Adv. Mater.* **2024**, *36*, 2312564. [CrossRef]
21. Almohammadi, H.; Khadem, S.A.; Azzari, P.; Yuan, Y.; Guerra, A.; Rey, A.D.; Mezzenga, R. Liquid–liquid crystalline phase separation of filamentous colloids and semiflexible polymers: Experiments, theory and simulations. *Rep. Prog. Phys.* **2025**, *88*, 036601. [CrossRef] [PubMed]
22. Almohammadi, H.; Fu, Y.; Mezzenga, R. Evaporation-Driven Liquid–Liquid Crystalline Phase Separation in Droplets of Anisotropic Colloids. *ACS Nano* **2023**, *17*, 3098–3106. [CrossRef]
23. Azzari, P.; Bagnani, M.; Mezzenga, R. Liquid–liquid crystalline phase separation in biological filamentous colloids: Nucleation, growth and order–order transitions of cholesteric tactoids. *Soft Matter* **2021**, *17*, 6627–6636. [CrossRef] [PubMed]
24. Deegan, R.D.; Bakajin, O.; Dupont, T.F.; Huber, G.; Nagel, S.R.; Witten, T.A. Capillary flow as the cause of ring stains from dried liquid drops. *Nature* **1997**, *389*, 827–829, Erratum in *Nature* **2021,** *592,* E12. [CrossRef]
25. McBride, S.A.; Dash, S.; Khan, S.; Varanasi, K.K. Evaporative Crystallization of Spirals. *Langmuir* **2019**, *35*, 10484–10490. [CrossRef]
26. Carrithers, A.D.; Brown, M.J.V.I.; Rashed, M.Z.; Islam, S.; Velev, O.D.; Williams, S.J. Multiscale Self-Assembly of Distinctive Weblike Structures from Evaporated Drops of Dilute American Whiskeys. *ACS Nano* **2020**, *14*, 5417–5425. [CrossRef]
27. Xu, J.; Xia, J.; Hong, S.W.; Lin, Z.; Qiu, F.; Yang, Y. Self-Assembly of Gradient Concentric Rings via Solvent Evaporation from a Capillary Bridge. *Phys. Rev. Lett.* **2006**, *96*, 066104. [CrossRef]

28. Sáenz, P.J.; Wray, A.W.; Che, Z.; Matar, O.K.; Valluri, P.; Kim, J.; Sefiane, K. Dynamics and universal scaling law in geometrically-controlled sessile drop evaporation. *Nat. Commun.* **2017**, *8*, 14783. [CrossRef]
29. Safdari, M.; Zandi, R.; van der Schoot, P. Effect of electric fields on the director field and shape of nematic tactoids. *Phys. Rev. E* **2021**, *103*, 062703. [CrossRef]
30. Huang, X.; Zacharia, N.S. Functional polyelectrolyte multilayer assemblies for surfaces with controlled wetting behavior. *J. Appl. Polym. Sci.* **2015**, *132*, 42767. [CrossRef]
31. Park, S.M.; Bagnani, M.; Yun, H.S.; Han, M.J.; Mezzenga, R.; Yoon, D.K. Hierarchically fabricated amyloid fibers via evaporation-induced self-assembly. *ACS Nano* **2021**, *15*, 20261–20266. [CrossRef]
32. Shao, X.; Duan, F.; Hou, Y.; Zhong, X. Role of surfactant in controlling the deposition pattern of a particle-laden droplet: Fundamentals and strategies. *Adv. Colloid. Interface Sci.* **2020**, *275*, 102049. [CrossRef] [PubMed]
33. Lin, D.; Wang, S.; Xu, W.; Chen, Y.; Li, P.; Fang, Y.-G.; Zhao, W.; Duan, X.; Yang, X.; Jiang, Z.; et al. Topological wetting states of microdroplets on closed-loop structured surfaces: Breakdown of the Gibbs equation at the microscale. *Proc. Natl. Acad. Sci. USA* **2024**, *121*, e2315730121. [CrossRef] [PubMed]
34. Zang, D.; Tarafdar, S.; Tarasevich, Y.Y.; Dutta Choudhury, M.; Dutta, T. Evaporation of a Droplet: From physics to applications. *Phys. Rep.* **2019**, *804*, 1–56. [CrossRef]
35. Majumder, M.; Rendall, C.S.; Eukel, J.A.; Wang, J.Y.L.; Behabtu, N.; Pint, C.L.; Liu, T.-Y.; Orbaek, A.W.; Mirri, F.; Nam, J.; et al. Overcoming the "Coffee-Stain" Effect by Compositional Marangoni-Flow-Assisted Drop-Drying. *J. Phys. Chem. B* **2012**, *116*, 6536–6542. [CrossRef]
36. Picknett, R.G.; Bexon, R. The evaporation of sessile or pendant drops in still air. *J. Colloid Interface Sci.* **1977**, *61*, 336–350. [CrossRef]
37. Patil, N.D.; Bange, P.G.; Bhardwaj, R.; Sharma, A. Effects of Substrate Heating and Wettability on Evaporation Dynamics and Deposition Patterns for a Sessile Water Droplet Containing Colloidal Particles. *Langmuir* **2016**, *32*, 11958–11972. [CrossRef]
38. Dignon, G.L.; Best, R.B.; Mittal, J. Biomolecular Phase Separation: From Molecular Driving Forces to Macroscopic Properties. *Annu. Rev. Phys. Chem.* **2020**, *71*, 53–75. [CrossRef]
39. Alberti, S.; Gladfelter, A.; Mittag, T. Considerations and Challenges in Studying Liquid-Liquid Phase Separation and Biomolecular Condensates. *Cell* **2019**, *176*, 419–434. [CrossRef]
40. Fraccia, T.P.; Zanchetta, G. Liquid–liquid crystalline phase separation in biomolecular solutions. *Curr. Opin. Colloid Interface Sci.* **2021**, *56*, 101500. [CrossRef]
41. Azzari, P.; Mezzenga, R. LLPS vs. *LLCPS*: Analogies and differences. *Soft Matter* **2023**, *19*, 1873–1881. [CrossRef] [PubMed]
42. Flory, P.J. *Principles of Polymer Chemistry*; Cornell University Press: Ithaca, NY, USA, 1953; pp. 514–544.
43. Rubinstein, R.; Colby, R.H. *Polymer Physics*; Oxford University Press: New York, NY, USA, 2003; Volume 23.
44. Onsager, L. The effects of shape on the interaction of colloidal particles. *Ann. N. Y. Acad. Sci.* **1949**, *51*, 627–659. [CrossRef]
45. Prost, J.; de Gennes, P.G. *The Physics of Liquid Crystals*; Oxford University Press: New York, NY, USA, 1993.
46. Nyström, G.; Arcari, M.; Mezzenga, R. Confinement-induced liquid crystalline transitions in amyloid fibril cholesteric tactoids. *Nat. Nanotechnol.* **2018**, *13*, 330–336. [CrossRef]
47. Lagerwall, J.P.F.; Schütz, C.; Salajkova, M.; Noh, J.; Hyun Park, J.; Scalia, G.; Bergström, L. Cellulose nanocrystal-based materials: From liquid crystal self-assembly and glass formation to multifunctional thin films. *NPG Asia Mater.* **2014**, *6*, e80. [CrossRef]
48. Wang, P.-X.; Hamad, W.Y.; MacLachlan, M.J. Structure and transformation of tactoids in cellulose nanocrystal suspensions. *Nat. Commun.* **2016**, *7*, 11515. [CrossRef]
49. Li, T.; Ilhamsyah, D.; Tai, B.; Shen, Y. Functional Biomaterials Derived from Protein Liquid–Liquid Phase Separation and Liquid-to-Solid Transition. *Adv. Mater.* **2025**, *37*, 2414703. [CrossRef]
50. Dignon, G.L.; Zheng, W.; Kim, Y.C.; Mittal, J. Temperature-Controlled Liquid–Liquid Phase Separation of Disordered Proteins. *ACS Cent. Sci.* **2019**, *5*, 821–830. [CrossRef]
51. Jin, X.; Zhou, M.; Chen, S.; Li, D.; Cao, X.; Liu, B. Effects of pH alterations on stress- and aging-induced protein phase separation. *Cell. Mol. Life Sci.* **2022**, *79*, 380. [CrossRef]
52. Lobaskin, V.; Qamhieh, K. Effective Macroion Charge and Stability of Highly Asymmetric Electrolytes at Various Salt Conditions. *J. Phys. Chem. B* **2003**, *107*, 8022–8029. [CrossRef]
53. Zhang, F.; Roosen-Runge, F.; Sauter, A.; Wolf, M.; Jacobs, R.M.J.; Schreiber, F. Reentrant condensation, liquid–liquid phase separation and crystallization in protein solutions induced by multivalent metal ions. *Pure Appl. Chem.* **2014**, *86*, 191–202. [CrossRef]
54. Ambadipudi, S.; Biernat, J.; Riedel, D.; Mandelkow, E.; Zweckstetter, M. Liquid–liquid phase separation of the microtubule-binding repeats of the Alzheimer-related protein Tau. *Nat. Commun.* **2017**, *8*, 275. [CrossRef]
55. Lin, Y.; Fichou, Y.; Longhini, A.P.; Llanes, L.C.; Yin, P.; Bazan, G.C.; Kosik, K.S.; Han, S. Liquid-Liquid Phase Separation of Tau Driven by Hydrophobic Interaction Facilitates Fibrillization of Tau. *J. Mol. Biol.* **2021**, *433*, 166731. [CrossRef]

56. Krainer, G.; Welsh, T.J.; Joseph, J.A.; Espinosa, J.R.; Wittmann, S.; de Csilléry, E.; Sridhar, A.; Toprakcioglu, Z.; Gudiškytė, G.; Czekalska, M.A.; et al. Reentrant liquid condensate phase of proteins is stabilized by hydrophobic and non-ionic interactions. *Nat. Commun.* **2021**, *12*, 1085. [CrossRef]
57. Guo, W.; Kinghorn, A.B.; Zhang, Y.; Li, Q.; Poonam, A.D.; Tanner, J.A.; Shum, H.C. Non-associative phase separation in an evaporating droplet as a model for prebiotic compartmentalization. *Nat. Commun.* **2021**, *12*, 3194. [CrossRef]
58. Othman, A.M.; Poulos, A.S.; Torres, O.; Routh, A.F. Liquid–Liquid Phase Separation Induced by Vapor Transfer in Evaporative Binary Sessile Droplets. *Langmuir* **2023**, *39*, 13242–13257. [CrossRef]
59. Chao, Y.; Ramírez-Soto, O.; Bahr, C.; Karpitschka, S. How liquid–liquid phase separation induces active spreading. *Proc. Natl. Acad. Sci. USA* **2022**, *119*, e2203510119. [CrossRef] [PubMed]
60. Kusumoto, Y.; Lomakin, A.; Teplow, D.B.; Benedek, G.B. Temperature dependence of amyloid β-protein fibrillization. *Proc. Natl. Acad. Sci. USA* **1998**, *95*, 12277–12282. [CrossRef] [PubMed]
61. Knowles, T.P.J.; Shu, W.; Devlin, G.L.; Meehan, S.; Auer, S.; Dobson, C.M.; Welland, M.E. Kinetics and thermodynamics of amyloid formation from direct measurements of fluctuations in fibril mass. *Proc. Natl. Acad. Sci. USA* **2007**, *104*, 10016–10021. [CrossRef]
62. Wetzel, R. Kinetics and Thermodynamics of Amyloid Fibril Assembly. *Acc. Chem. Res.* **2006**, *39*, 671–679. [CrossRef]
63. Liu, L. The Oseen-Frank Theory of Liquid Crystals. Ph.D. Thesis, University of Oxford, Oxford, UK, 2019.
64. Bagnani, M.; Nyström, G.; De Michele, C.; Mezzenga, R. Amyloid Fibrils Length Controls Shape and Structure of Nematic and Cholesteric Tactoids. *ACS Nano* **2019**, *13*, 591–600. [CrossRef]
65. Yunker, P.J.; Still, T.; Lohr, M.A.; Yodh, A.G. Suppression of the coffee-ring effect by shape-dependent capillary interactions. *Nature* **2011**, *476*, 308–311. [CrossRef]
66. Scriven, L.E.; Sternling, C.V. The Marangoni Effects. *Nature* **1960**, *187*, 186–188. [CrossRef]
67. Hu, H.; Larson, R.G. Analysis of the Effects of Marangoni Stresses on the Microflow in an Evaporating Sessile Droplet. *Langmuir* **2005**, *21*, 3972–3980. [CrossRef] [PubMed]
68. Jung, J.-M.; Gunes, D.Z.; Mezzenga, R. Interfacial Activity and Interfacial Shear Rheology of Native β-Lactoglobulin Monomers and Their Heat-Induced Fibers. *Langmuir* **2010**, *26*, 15366–15375. [CrossRef] [PubMed]
69. Gerber, J.; Schutzius, T.M.; Poulikakos, D. Patterning of colloidal droplet deposits on soft materials. *J. Fluid Mech.* **2021**, *907*, A39. [CrossRef]
70. Li, Y.; Yang, Q.; Li, M.; Song, Y. Rate-dependent interface capture beyond the coffee-ring effect. *Sci. Rep.* **2016**, *6*, 24628.
71. Accardo, A.; Shalabaeva, V.; Di Cola, E.; Burghammer, M.; Krahne, R.; Riekel, C.; Dante, S. Superhydrophobic Surfaces Boost Fibril Self-Assembly of Amyloid β Peptides. *ACS Appl. Mater. Interfaces* **2015**, *7*, 20875–20884. [CrossRef]
72. Bonn, D.; Eggers, J.; Indekeu, J.; Meunier, J.; Rolley, E. Wetting and spreading. *Rev. Mod. Phys.* **2009**, *81*, 739–805. [CrossRef]
73. Sárkány, Z.; Rocha, F.; Bratek-Skicki, A.; Tompa, P.; Macedo-Ribeiro, S.; Martins, P.M. Quantification of Surface Tension Effects and Nucleation-and-Growth Rates during Self-Assembly of Biological Condensates. *Adv. Sci.* **2023**, *10*, 2301501. [CrossRef]
74. Visser, B.S.; Lipiński, W.P.; Spruijt, E. The role of biomolecular condensates in protein aggregation. *Nat. Rev. Chem.* **2024**, *8*, 686–700. [CrossRef]
75. Lee, S.; A, M.T.; Cho, G.; Lee, J. Control of the Drying Patterns for Complex Colloidal Solutions and Their Applications. *Nanomaterials* **2022**, *12*, 2600. [CrossRef]
76. Wang, F.; Wu, Y.; Nestler, B. Wetting Effect on Patterned Substrates. *Adv. Mater.* **2023**, *35*, 2210745. [CrossRef]
77. Qi, C.; Ma, X.; Zeng, Q.; Huang, Z.; Zhang, S.; Deng, X.; Kong, T.; Liu, Z. Multicompartmental coacervate-based protocell by spontaneous droplet evaporation. *Nat. Commun.* **2024**, *15*, 1107. [CrossRef]
78. Xia, D.; Johnson, L.M.; López, G.P. Anisotropic Wetting Surfaces with One-Dimesional and Directional Structures: Fabrication Approaches, Wetting Properties and Potential Applications. *Adv. Mater.* **2012**, *24*, 1287–1302. [CrossRef] [PubMed]
79. Banerjee, I.; Pangule, R.C.; Kane, R.S. Antifouling Coatings: Recent Developments in the Design of Surfaces That Prevent Fouling by Proteins, Bacteria, and Marine Organisms. *Adv. Mater.* **2011**, *23*, 690–718. [CrossRef] [PubMed]
80. Prime, K.L.; Whitesides, G.M. Self-Assembled Organic Monolayers: Model Systems for Studying Adsorption of Proteins at Aurfaces. *Science* **1991**, *252*, 1164–1167. [CrossRef] [PubMed]
81. Ostuni, E.; Chapman, R.G.; Holmlin, R.E.; Takayama, S.; Whitesides, G.M. A Survey of Structure−Property Relationships of Surfaces that Resist the Adsorption of Protein. *Langmuir* **2001**, *17*, 5605–5620. [CrossRef]
82. Zhang, Z.; Deng, C.; Fan, X.; Li, M.; Zhang, M.; Wang, X.; Chen, F.; Shi, S.; Zhou, Y.; Deng, L.; et al. 3D Directional Assembly of Liquid Crystal Molecules. *Adv. Mater.* **2024**, *36*, 2401533. [CrossRef]
83. Martchenko, I.; Crassous, J.J.; Mihut, A.M.; Bialik, E.; Hirt, A.M.; Rufier, C.; Menzel, A.; Dietsch, H.; Linse, P.; Schurtenberger, P. Anisotropic magnetic particles in a magnetic field. *Soft Matter* **2016**, *12*, 8755–8767. [CrossRef]
84. Swan, J.W.; Bauer, J.L.; Liu, Y.; Furst, E.M. Directed colloidal self-assembly in toggled magnetic fields. *Soft Matter* **2014**, *10*, 1102–1109. [CrossRef]
85. Li, Y.; He, L.; Zhang, X.; Zhang, N.; Tian, D. External-Field-Induced Gradient Wetting for Controllable Liquid Transport: From Movement on the Surface to Penetration into the Surface. *Adv. Mater.* **2017**, *29*, 1703802. [CrossRef]

86. Zhang, L.; Sun, L.; Zhang, Z.; Wang, Y.; Yang, Z.; Liu, C.; Li, Z.; Zhao, Y. Bioinspired superhydrophobic surface by hierarchically colloidal assembling of microparticles and colloidal nanoparticles. *Chem. Eng. J.* **2020**, *394*, 125008. [CrossRef]
87. Park, S.M.; Park, G.; Cha, Y.J.; Yoon, D.K. Generation of 2D DNA Microstructures via Topographic Control and Shearing. *Small* **2020**, *16*, 2002449. [CrossRef]
88. Iqbal, M.; Dinh, D.K.; Abbas, Q.; Imran, M.; Sattar, H.; Ul Ahmad, A. Controlled Surface Wettability by Plasma Polymer Surface Modification. *Surfaces* **2019**, *2*, 349–371. [CrossRef]
89. Latip, E.A.; Coudron, L.; McDonnell, M.; Johnston, I.; McCluskey, D.; Day, R.; Tracey, M. Protein droplet actuation on superhydrophobic surfaces: A new approach toward anti-biofouling electrowetting systems. *RSC Adv.* **2017**, *7*, 49633–49648. [CrossRef]
90. Knowles, T.P.; Fitzpatrick, A.W.; Meehan, S.; Mott, H.R.; Vendruscolo, M.; Dobson, C.M.; Welland, M.E. Role of Intermolecular Forces in Defining Material Properties of Protein Nanofibrils. *Science* **2007**, *318*, 1900–1903. [CrossRef]
91. Fitzpatrick, A.W.P.; Debelouchina, G.T.; Bayro, M.J.; Clare, D.K.; Caporini, M.A.; Bajaj, V.S.; Jaroniec, C.P.; Wang, L.; Ladizhansky, V.; Müller, S.A.; et al. Atomic structure and hierarchical assembly of a cross-β amyloid fibril. *Proc. Natl. Acad. Sci. USA* **2013**, *110*, 5468–5473. [CrossRef]
92. Jordens, S.; Riley, E.E.; Usov, I.; Isa, L.; Olmsted, P.D.; Mezzenga, R. Adsorption at Liquid Interfaces Induces Amyloid Fibril Bending and Ring Formation. *ACS Nano* **2014**, *8*, 11071–11079. [CrossRef]
93. Chai, Z.; Childress, A.; Busnaina, A.A. Directed Assembly of Nanomaterials for Making Nanoscale Devices and Structures: Mechanisms and Applications. *ACS Nano* **2022**, *16*, 17641–17686. [CrossRef]
94. Ma, J.; Lin, S.; Jiang, Y.; Li, P.; Zhang, H.; Xu, Z.; Wu, H.; Lin, P.; Breu, J.; Gao, W.; et al. Digital Programming Graphene Oxide Liquid Crystalline Hybrid Hydrogel by Shearing Microlithography. *ACS Nano* **2020**, *14*, 2336–2344. [CrossRef]
95. Mirri, G.; Škarabot, M.; Muševič, I. In situ laser-imprinted surface realignment of a nematic liquid crystal. *Soft Matter* **2015**, *11*, 3347–3353. [CrossRef] [PubMed]
96. Jampani, V.; SǩarabotM.; Takezoe, H.; Muševič, I.; Dhara, S. Laser-driven microflow-induced bistable orientation of a nematic liquid crystal in perfluoropolymer-treated unrubbed cells. *Opt. Express* **2013**, *21*, 724–729. [CrossRef] [PubMed]
97. Shen, Y.; Posavec, L.; Bolisetty, S.; Hilty, F.M.; Nyström, G.; Kohlbrecher, J.; Hilbe, M.; Rossi, A.; Baumgartner, J.; Zimmermann, M.B.; et al. Amyloid fibril systems reduce, stabilize and deliver bioavailable nanosized iron. *Nat. Nanotechnol.* **2017**, *12*, 642–647. [CrossRef]
98. Han, Y.; Cao, Y.; Zhou, J.; Yao, Y.; Wu, X.; Bolisetty, S.; Diener, M.; Handschin, S.; Lu, C.; Mezzenga, R. Interfacial Electrostatic Self-Assembly of Amyloid Fibrils into Multifunctional Protein Films. *Adv. Sci.* **2023**, *10*, 2206867. [CrossRef] [PubMed]
99. Olsson, R.T.; Azizi Samir, M.A.; Salazar-Alvarez, G.; Belova, L.; Ström, V.; Berglund, L.A.; Ikkala, O.; Nogués, J.; Gedde, U.W. Making flexible magnetic aerogels and stiff magnetic nanopaper using cellulose nanofibrils as templates. *Nat. Nanotechnol.* **2010**, *5*, 584–588. [CrossRef]
100. Xia, Y.; Whitesides, G.M. Soft Lithography. *Angew. Chem. Int. Ed.* **1998**, *37*, 550–575. [CrossRef]
101. Young, T. An essay on the cohesion of fluids. *Abstr. Pap. Print. Philos. Trans. R. Soc. Lond.* **1997**, *1*, 171–172.
102. de Gennes, P.G. Wetting: Statics and dynamics. *Rev. Mod. Phys.* **1985**, *57*, 827–863. [CrossRef]
103. Coulson, S.R.; Woodward, I.; Badyal, J.P.S.; Brewer, S.A.; Willis, C. Super-Repellent Composite Fluoropolymer Surfaces. *J. Phys. Chem. B* **2000**, *104*, 8836–8840. [CrossRef]
104. Soeno, T.; Inokuchi, K.; Shiratori, S. Ultra-water-repellent surface: Fabrication of complicated structure of SiO_2 nanoparticles by electrostatic self-assembled films. *Appl. Surf. Sci.* **2004**, *237*, 539–543. [CrossRef]
105. Chen, W.; Fadeev, A.Y.; Hsieh, M.C.; Öner, D.; Youngblood, J.; McCarthy, T.J. Ultrahydrophobic and Ultralyophobic Surfaces: Some Comments and Examples. *Langmuir* **1999**, *15*, 3395–3399. [CrossRef]
106. Wang, X.; Li, Y.; Zhong, C. Amyloid-directed assembly of nanostructures and functional devices for bionanoelectronics. *J. Mater. Chem. B* **2015**, *3*, 4953–4958. [CrossRef]
107. Bolisetty, S.; Boddupalli, C.S.; Handschin, S.; Chaitanya, K.; Adamcik, J.; Saito, Y.; Manz, M.G.; Mezzenga, R. Amyloid Fibrils Enhance Transport of Metal Nanoparticles in Living Cells and Induced Cytotoxicity. *Biomacromolecules* **2014**, *15*, 2793–2799. [CrossRef]
108. Nyström, G.; Fernández-Ronco, M.P.; Bolisetty, S.; Mazzotti, M.; Mezzenga, R. Amyloid Templated Gold Aerogels. *Adv. Mater.* **2016**, *28*, 472–478. [CrossRef] [PubMed]
109. Gong, H.; Sakaguchi, Y.; Suzuki, T.; Yanagisawa, M.; Aida, T. Near-identical macromolecules spontaneously partition into concentric circles. *Nature* **2024**, *636*, 92–99. [CrossRef] [PubMed]
110. Jeihanipour, A.; Lahann, J. Deep-Learning-Assisted Stratification of Amyloid Beta Mutants Using Drying Droplet Patterns. *Adv. Mater.* **2022**, *34*, 2110404. [CrossRef] [PubMed]
111. Abbas, M.; Law, J.O.; Grellscheid, S.N.; Huck, W.T.S.; Spruijt, E. Peptide-Based Coacervate-Core Vesicles with Semipermeable Membranes. *Adv. Mater.* **2022**, *34*, 2202913. [CrossRef]
112. Ji, Y.; Lin, Y.; Qiao, Y. Plant Cell-Inspired Membranization of Coacervate Protocells with a Structured Polysaccharide Layer. *J. Am. Chem. Soc.* **2023**, *145*, 12576–12585. [CrossRef]

113. Gao, N.; Xu, C.; Yin, Z.; Li, M.; Mann, S. Triggerable Protocell Capture in Nanoparticle-Caged Coacervate Microdroplets. *J. Am. Chem. Soc.* **2022**, *144*, 3855–3862. [CrossRef]
114. Shao, J.; Luo, Y.; Wu, H.; Wang, J.; Zhou, X.; Er, S.; Cao, S.; Sun, H.; Pérez Garza, H.H.; Zheng, H.; et al. Designing polymersomes with surface-integrated nanoparticles through hierarchical phase separation. *Nat. Commun.* **2025**, *16*, 2445. [CrossRef]
115. Mason, A.F.; Buddingh', B.C.; Williams, D.S.; van Hest, J.C.M. Hierarchical Self-Assembly of a Copolymer-Stabilized Coacervate Protocell. *J. Am. Chem. Soc.* **2017**, *139*, 17309–17312. [CrossRef]
116. Javed, S.; Spruijt, E. Resilient Membranized Coacervates Formed through Spontaneous Wrapping of Heat-Destabilized Lipid Bilayers around Coacervate Droplets. *Adv. Sci.* **2025**, *12*, 2412312. [CrossRef]
117. Bi, S.; Yang, C.; Zhang, W.; Xu, J.; Liu, L.; Wu, D.; Wang, X.; Han, Y.; Liang, Q.; Zhang, F. Two-dimensional semiconducting covalent organic frameworks via condensation at arylmethyl carbon atoms. *Nat. Commun.* **2019**, *10*, 2467. [CrossRef]
118. Shu, R.; Xu, Y.; Fei, J.; Yu, F.; Li, Z.; Meng, X.; Li, J. Artificial Chloroplast Nanoarchitectonics through Liquid–Liquid Phase Separation Enables Recycled and Enhanced Photosynthesis. *J. Am. Chem. Soc.* **2025**, *147*, 27011–27019. [CrossRef]
119. Wang, T.; Fei, J.; Yu, F.; Xu, X.; Cui, Y.; Li, J. Nanoarchitectonics of Vesicle Microreactors for Oscillating ATP Synthesis and Hydrolysis. *Angew. Chem. Int. Ed.* **2024**, *63*, e202411981. [CrossRef]
120. Song, S.; Ivanov, T.; Yuan, D.; Wang, J.; da Silva, L.C.; Xie, J.; Cao, S. Peptide-Based Biomimetic Condensates via Liquid–Liquid Phase Separation as Biomedical Delivery Vehicles. *Biomacromolecules* **2024**, *25*, 5468–5488. [CrossRef]

Disclaimer/Publisher's Note: The statements, opinions and data contained in all publications are solely those of the individual author(s) and contributor(s) and not of MDPI and/or the editor(s). MDPI and/or the editor(s) disclaim responsibility for any injury to people or property resulting from any ideas, methods, instructions or products referred to in the content.